THE UNIVERSITY OF CHICAGO

EXPLORING THE SENSORY INNERVATION OF THE LARVAL ZEBRAFISH PECTORAL FIN

A DISSERTATION SUBMITTED TO
THE FACULTY OF THE DIVISION OF THE BIOLOGICAL SCIENCES
AND THE PRITZKER SCHOOL OF MEDICINE
IN CANDIDACY FOR THE DEGREE OF
DOCTOR OF PHILOSOPHY

GRADUATE PROGRAM IN INTEGRATIVE BIOLOGY

BY
KATHARINE WEBSTER HENDERSON

CHICAGO, ILLINOIS
DECEMBER 2020

For Weedie (1984 - 2012)

TABLE OF CONTENTS

LIST OF FIGURES

LIST OF TABLES

ACKNOWLEDGMENTS

Thank you to the funding agencies and research resources that made this work, well, work. This material was supported by the National Science Foundation Graduate Research Fellowship under Grant No. DGE-1144082 & DGE-1746045, the Office of Naval Research Department of Defense grant N00014-18-1-2673, and U. S. Department of Education Graduate Assistance in Areas of National Need P200a150077. Part of this work was completed with resources provided by the University of Chicago Research Computing Center. Imaging (and/or image processing and/or data analysis) was performed at the University of Chicago Integrated Light Microscopy Facility. I thank Dr. Christine Labno in particular for her assistance with microscopy training, general imaging approaches, Fiji, and the occasional redundant question.

Thank you to the people who made this project possible. Like many dissertations, this project started with one goal and ended up addressing something slightly different. Along the way, my committee helped steer my course and keep me on track. Thank you to all my scientific advisors. To Melina Hale for mentoring me all these years, and thank you for keeping me grounded. To Sliman Bensmaia, Ruth Anne Eatock, and Vicky Prince for always pushing my science to the next level and encouraging me to think deeply about my findings. To Evi Menelaou for throwing me a life preserver when I needed one most. To Adam Hardy, Brett Aiello, and Hilary Katz for keeping the student space fun and engaging. To the folks in the Department of Organismal Biology and Anatomy, Audrey Aronowsky, Cindy King, Dale Janeczko, America Barrera, and Annetha Bartley, thank you for keeping the wheels turning.

Thank you to my family who taught me everything I know. To my grandparents for supporting my pursuit of education every step of the way. To Aunt Jean, Uncle Mike, Aunt Jan, and AJ for being patient and kind while I chased my dreams. To my mom for showing me what integrity and dedication look like. To my chosen family, who keep me going: Broussie for always seeing me, Shmee Shmoo for always believing, Yan for incredible tenderness, Sama for conversations both lighthearted and thoughtful, Natalia for always meeting me where I'm at, Dacy for making me soup, Jesse and Rebecca for much needed recuperation, Jackie for being a friend in a dark

night, Ximena for never giving up hope, Marcin for every catch and inspired conversation, Lance and Ashley for the porch parties, and Dave for teaching me the depth of partnership. Thank you to my dog, Shenzi, for reminding me to float. Finally, thank you to my brother Will for inspiring my curiosity.

ABSTRACT

Sensory neurons in the skin provide critical input for animal movement and a wide range of behaviors. In this thesis, I analyze the pectoral fin sensory neurons of larval zebrafish with a focus on the detailed anatomy of individual neurons that innervate the fins. In chapter 2, this work shows, for the first time, that the cell bodies of pectoral fin sensory neurons are located in both the hindbrain and the spinal cord. Single cell reconstructions of the entire primary afferent arborization revealed that many fin neurons branch widely across the fin and, in many cases, innervate both medial and lateral surfaces as well as the surface of the axial trunk adjacent to the fin. Fin sensory neurons exhibit four distinct soma morphologies, but they do not have any somatotopy with respect to fin regions. Agglomerative hierarchical clustering analysis reveals that the entire population of fin sensory neurons fall into three distinct clusters based on morphological parameters, suggesting possible subtypes. In chapter 3, I next examined the full sensory innervation of the fin's surface to better understand the fin as a sensory structure. In order to do this, I quantified the terminal distributions for the whole population of fin sensory neurons and dorsal root ganglia neurons innervating the fin structure. Comparison between full population-labeled and stochastically labeled individual neurons suggests that the stochastic labeling approach under sampled innervation of the lateral fin surface. By examining distances between nearest neighbor neuron endings, I found that single cells tended to innervate the fin in an organized fashion that prioritized filling space while self-avoiding whereas the whole population did not. Finally, terminal distributions at two locations of functional importance to sensation and movement, the fin membrane margin and the blood vessel, are not notably different from a control transect in the membrane, indicating a lack of functional specificity of terminal distributions. However, the density of terminals at the fin membrane margin is significantly higher than at the blood vessel. Taken together, the results presented in this thesis establish the neuroanatomy, including terminal distributions, of a tractable *in vivo* model that can be utilized for both anatomical and functional studies of a whole limb sensory system.

CHAPTER 1

INTRODUCTION

Animals rely on input from primary sensory afferents in their skin in order to modulate their internal homeostasis and navigate their external environments. Considerable previous research has documented a wide range of sensory receptors and nerve ending in the skin of diverse animals from tetrapods to invertebrates (e.g. [123, 25, 21] reviewed in [103]). While the anatomy of sensors in the skin has been described through histology and other ultrastructure analysis, there is little that is known about the underlying neuroanatomy of the whole cells. Sectioning, labeling, and analyzing samples of surface tissue is quite a bit more straightforward than tracing the paths of neuron branches from the cell body to those endings. Furthermore, an in-depth examination of the entire terminal population of a whole limb has not been conducted before. This is likely due to the fact that assessing large areas of skin with traditional approaches and at the single cell level is impractical and mapping the limb by reconstructing the full skin surface section-by section in an individual is not currently feasible.

1.1 Whole cell reconstructions provide insights into neuroanatomy

Classical neuroscience studies relied heavily on staining single neurons and examining their structure. Indeed, the foundation of modern neurobiology can be traced back to the work of Camillo Golgi and Santiago Ramón y Cajal. In 1873, Golgi created the "reazione nera:" this "black reaction" using silver nitrate randomly labeled neurons and glia in the central nervous system [35]. Commonly referred to today as the Golgi method, this technique revolutionized scientific inquiry in the field of neurobiology. Golgi himself utilized the method to describe a number of structures in the central nervous system [36, 37, 38]. This staining approach and in-depth neuroanatomical examinations uniquely allowed for the identification of individual neurons. Perhaps most significantly, Ramón y Cajal eventually adopted Golgi's technique to investigate individual neurons, and, as a result, he identified dendritic spines and theorized a new approach to ner-

vous system function. This theory proposed that the central nervous system was composed not of continuous tissues, as was commonly thought, but instead by interconnected individual cells [116, 117, 118] reviewed in [27]. All of this foundational work was possible through the use of the Golgi method and neuroanatomical examination.

More recently, classical neuroanatomical techniques have been replaced by a number of technological improvements allowing for more directed anatomical explorations. Chief among these improvements are modernized genetic toolkits that allow for targeted single cell labeling with minimal disruption of the surrounding tissues, advanced microscopy technologies with long working distance high numerical aperture objectives, and significant improvements in computational power providing the capacity to examine and process massive image files. Genetic tools [50, 8, 28, 5, 6, 89, 51], transsynaptic tracing techniques [147, 159, 161], and optogenetics [68] allow labeling and silencing of sensory neuron subtypes, mapping of neural circuits, and assessment of their functional roles in behavior. Through innovative and combinatorial experimental paradigms, it is now possible to study model organisms with improved cellular resolution and in more biologically relevant contexts [22, 57, 71].

Recent neuroanatomical studies in zebrafish have deepened our understanding of the spinal cord. These studies have benefitted from improved imaging approaches including scanning, tiling, and stitching, all of which have expanded the depth of *in vivo* interrogation in this optically transparent and small vertebrate model system. These features, together with the zebrafish's genetic toolkit, allow for unprecedented access to the whole, intact nervous system *in vivo*. Classical zebrafish studies utilized horseradish peroxidase to provide retrograde labeling of reticulospinal neurons [69]. More recent work in zebrafish has identified subsets of spinal interneurons based on retrograde labeling with modern fluorescent molecules [45, 20]. These neuroanatomical studies can eventually be combined with functional investigations to link neuroanatomy to function [90]. Through these investigations, our understanding of the morphology and function of the central nervous system of zebrafish has improved.

1.2 The pectoral fins of fish as a model for limb systems

The pectoral fins of actinopterygian fishes have been the subject of a number of studies in the field of evolutionary developmental biology, and they are a useful model system with which to examine homology across evolution [98, 34]. Like the tetrapod forelimb, the pectoral fins are paired appendages situated anteriorly on the trunk of the vertebrate body plan. Exploration through the field of evolutionary developmental biology has revealed that expression of the underlying Hox genes regulating forelimb development has shifted more posteriorly through evolution [113, 138, 87, 24]. The developmental similarities in forelimb planning suggests that forelimb features are conserved through evolution. As a result, the pectoral fins of fishes, homologs to the tetrapod forelimb, provide an interesting playground within which to explore vertebrate limb sensory systems.

Prior work in a variety of fish species has established that pectoral fins of adult fish are capable of proprioceptive, somatosensory, and chemosensory feedback. Early work in sea robins indicated that free fin rays of adults are capable of chemosensory feedback [135]. Adults of another benthic species, which live close to the substrate and frequently interact with surfaces, have been shown to possess highly innervated fin rays that respond to pressure [47]. In adult fish that live in the water column, pectoral fins contain both rapidly and slowly adapting mechanosensors [151, 4]. In experimental manipulations ablating sensory feedback from fins, Williams and Hale observed a decrease in locomotor function [150]. While these studies provided key insights into the function of pectoral fins as sensors, adult fishes are not a tractable system in which to examine whole sensory neurons in their entirety. Larval zebrafish, however, are small and transparent, thus making them an easily accessible model system that holds promise to examine the pectoral fin and its associated neuroanatomy.

1.3 The pectoral fins of fish undergo significant remodeling through early ontogeny

At 5 days post fertilization (dpf), the pectoral fins of larval zebrafish have developed into a two-part structure that includes the fin body (FB) and the fin membrane (FM). The FB is composed of an endochondrial disk layered on the medial and lateral sides with simple adductor and abductor muscle fibers extending in a fan from the proximal to distal end of the FB [39, 143]. The FM is comprised of the actinotrichia, which eventually give rise to the fin rays in adult zebrafish [39, 143]. The FB of the pectoral fin is innervated by a pool of motor neurons that crosses the anatomical transition area between the hindbrain and the spinal cord [87, 24, 138, 113], a stark contrast to the mammalian forelimb motor pool that is restricted to the spinal cord. The pectoral fin remains in this "larval state" until the juvenile stages [39].

During this time in development, larval zebrafish exhibit bilateral pectoral fin abduction while initiating forward swimming bouts [41]. By 5dpf, they are capable of predatory strikes, escape maneuvers, as well as slow swimming behaviors. Once moving forward in a slow swim bout, larval zebrafish continue to beat their pectoral fins; however, there is no association between fin beat frequency and swimming speed [41]. In experiments comparing the kinematics of finless larval zebrafish morphants to wild type larvae, Green et al. found that there was no difference in speed or duration of slow swim bouts [41]. While the pectoral fins of larval zebrafish are active during locomotion, this work suggests that they do not function to generate appreciable force for locomotor initiation, ongoing propulsion, or stabilization, raising the question of whether or not they incorporate mechanosensory feedback. As larval zebrafish progress through the late larval stages, the fin continuously adds muscle fibers to both adductors and abductors, approximately doubling their muscle fiber numbers [108].

Following this period of hyperplasia and hypertrophy, the larval zebrafish pectoral fin begins to undergo more substantial changes during the juvenile stages [143]. This time period, corresponding to about 20 to 23dpf, sees a complete rotation of the fin from a vertical orientation to

horizontal orientation with reference to the body axis (Fig. 1.1) [39, 143]. The fin rays also finish ossifying, a characteristic that is a key structural element of the adult pectoral fin [143]. Importantly, the simple musculature of the FB at the larval and early juvenile stages takes on the adult morphology composed of three complementary adductor and abductor pairs [143]. At this point, the fin is capable of the more subtle locomotor function of the adult. During adult stages, the fin is functionally and anatomically distinct from the larval stages. In adult fishes, the pectoral fin is primarily a locomotor structure, as is true of most tetrapod forelimbs.

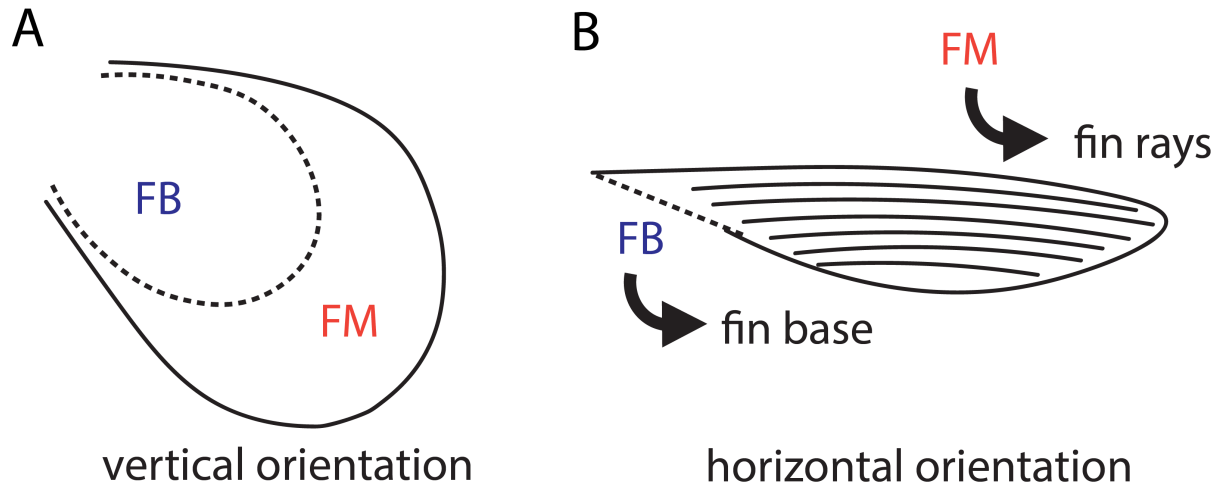

Figure 1.1: Schematic of larval vs. adult fins. (A) The pectoral fins at the larval stage are positioned in a vertical orientation. The fin is composed of the fin body (dotted line, FB) and the fin membrane (FM). (B) By adult stages, the pectoral fin has moved into a horizontal position, and the FB has become the base of the fin (dotted line), and the FM has given rise to the fin rays in the fin itself (horizontal lines). Anterior is to the left, dorsal is up.

A clear role for the sensory innervation of the pectoral fins in larval zebrafish has not been identified. Despite the well-established evidence for mechanosensory feedback in the pectoral fins of adult fishes, anecdotal evidence from both behavioral and physiological experiments in the Hale Lab has not supported a mechanosensory function for larval zebrafish pectoral fins. There is, however, evidence for a respiratory function of larval zebrafish fins. Post-hatch, larval zebrafish utilize cutaneous respiration before their gills become functional at around 21dpf [125]. Early studies showed that the spontaneous bouts of forward swimming movement of larval fishes increase in low oxygen environments [59, 146]. Functional studies altering oxygen concentrations

have shown that larval fish increase their fin beats in the presence of low oxygen [41, 61, 64, 65]. On top of that, there is a marked decrease in fluid mixing around the anterior portion of the body when the fins are not adducted [41]. In depth modeling of pectoral fin bending and fluid mixing has also revealed that the "joint" between the FB and the FM is ideally positioned to maximize fluid mixing around the head and anterior body axis [40]. These results, combined with the lack of compelling evidence for mechanosensory function of larval zebrafish pectoral fins, suggest that the pectoral fins at pre-juvenile stages may in fact serve a respiratory function.

1.4 Larval zebrafish possess centrally located primary sensors innervating the skin

Aquatic vertebrates possess a unique class of sensory neurons that are found in the central nervous system. These intraspinal sensory neurons are called Rohon-Beard neurons (RBs), and they were initially described in the late 1800s in *Xenopus laevis* [124, 17, 123]. These sensory neurons, with their cell bodies located in the central nervous system, are complemented by the dorsal root ganglia neurons (DRG neurons) located in the peripheral nervous system. Recent studies incorporating novel techniques have led to a more nuanced view of these neurons and their synaptic partners within spinal circuits.

RBs are now known to be present in a number of aquatic species. They are a transient population of neurons present during early life history before development of sensory neurons in the dorsal root ganglia [77, 99, 52, 53, 120]. RBs are located in the dorsal spinal cord and exhibit a broad spectrum of primary afferent branching patterns in the skin [123, 25, 91]. Initial functional studies identified RBs as mechanosensors that respond to touch on the skin in *X. laevis* [123, 25]. The classical views of RB function is that these glutamatergic cells mediate initiation of motor output in response to tactile stimulation [25, 83]. While axial RBs are undoubtedly mechanosensory, recent work has also begun to explore additional sensory modalities within this cell type.

While RBs were traditionally thought to be a homogeneous population [123, 134], recent ex-

periments have identified subpopulations of RBs with different ion channel compositions and gene expression patterns [110, 75, 104]. The heterogeneity of ion channels, specifically the expression of different classes of sodium channels, suggests differences in sensory roles across the RB population [110]. Heterogeneity of gene expression has revealed subsets of RBs express mechanosensory *piezo2b*, a homolog to the stretch-activated *piezo2* in mammals [29], and others that express chemosensory transient receptor potential, trpA1 ion channels [114]. In mammalian systems, it is known that primary sensory cells of the dorsal root ganglia are separated into subtypes based on firing properties, mechanosensory ion channels, soma positions, and projections to the spinal cord [109, 80, 48, 81]. Taken together, the diversity of ion channels expressed in subtypes of RBs suggests that similar organizational principles might also exist for RBs in zebrafish and other aquatic organisms with RB subtypes responding to different sensory inputs. Zebrafish offer a unique opportunity to investigate *in vivo* how primary sensory signals are encoded by subtypes of sensory neurons in the spinal cord.

1.5 Larval zebrafish also possess peripheral sensory ganglia

Like all other vertebrates, larval zebrafish also possess dorsal root ganglia (DRG) neurons. Past hypotheses suggested that the timing of DRG neuron development also signaled RB apoptosis [58], but this is now understood to be de-coupled from RB cell death [120]. Indeed, the two neuron types overlap during mid to late larval stages [20, 149, 55]. By 48 hours post fertilization, the most anterior of the DRG neurons have begun to differentiate and migrate ventrally [115, 149]. Between two and half and three days post fertilization (dpf), larval zebrafish have at least one fully differentiated DRG neuron present at the level of the ventral root of each myomere along the entire body axis [20, 149]. The axons of DRG neurons and RBs together form the dorsal longitudinal fasciculus (DLF) [20]. While DRG neurons develop later in the post-embryonic stages, their anatomical distributions in each myomere and their projections mixing with RB axons suggest the possibility of similar targets within the spinal cord. DRG neurons steadily increase in number until there are over 100 neurons in a single ganglion at 28dpf [7].

1.6 Research focus and thesis organization

In my dissertation research, I examine sensory innervation of the pectoral fins in 5dpf larval zebrafish through the lens of whole limb innervation. Prior work has only been able to examine sensory innervation in reduced preparations. While this has proven insightful for exploring sensory structure piecemeal, we are now at a point where we can begin to explore the sensory structure of a whole limb system in its entirety. A baseline examination of the arborization of the larval fish pectoral fin will be critical for further investigations of the whole limb as a sensor that changes radically through metamorphosis. On top of that, general principles of sensorimotor organization can be explored in this tractable system.

In chapter two of this thesis, I examine the fin sensory neurons (FSNs) of 5dpf transgenic larval zebrafish. This chapter centers around the question: What is the population of neurons responsible for sensory innervation of the pectoral fins? Surprisingly, I identified that FSNs are a mixed population composed of RBs and a novel population of *islet2B*+ neurons located at the level of rhombomere 7/8 in the hindbrain. Across the 20 neuron sample, I used 10 morphological parameters and two cell body parameters to examine the inter-relatedness of the sampled population. Using agglomerative hierarchical clustering, I identify at least two subtypes of FSN with a possible third subtype identified as well. I explore the functional implications of innervation patterns within the fin, and I note that there is no somatotopy with regard to soma locations and fin innervation patterns. I do identify a strong trend between medial fin surface terminal numbers and axial terminal numbers in the area immediately under the fin.

In chapter three, I further delve into the pectoral fin as a sensory structure in and of itself. For this work, I extensively examined the *islet2B*+ terminals arising from both FSNs and DRG neurons. I examined two functionally relevant margins in the fin: the blood vessel bounding the muscle in the fin body and the fin margin at the very edge of the fin membrane. As a control, I also examined a midpoint on the membrane between the two margins. These regions encompass the functional "joint" that bends with fin adduction, the distal most point of the sensory structure, and a third intermediate point, respectively. I compare the entire sensory population to individual

cells to begin to untangle the representation of single neurons in the entire pectoral fin nervous innervation. I also establish distribution densities of terminals across the entire medial and lateral surfaces of the fin.

Finally, in my fourth chapter, I discuss my results and propose new directions for future work. I have identified that sensory neurons in the fin are composed of multiple populations, and I propose that there are functional subtypes of FSNs that are reflected by their neuroanatomy. Furthermore, the intermixing of FSNs and DRG neurons reflects functional overlap between the two populations. Both groups of cells are innervating the surface of the fin at this stage, and DRG neurons may indeed be adopting some of the sensory roles of the FSNs. I explore analyses of my dissertation results within the context of what is already known about vertebrate limb sensation more broadly, and I provide some suggestions for future neuroanatomical and functional studies.

CHAPTER 2

HINDBRAIN AND SPINAL CORD CONTRIBUTIONS TO THE SENSORY INNERVATION OF THE LARVAL ZEBRAFISH PECTORAL FIN

2.1 Abstract

Vertebrate forelimbs contain arrays of sensory neuron fibers that transmit signals from the skin to the nervous system. We used the genetic toolkit and optical clarity of the larval zebrafish to conduct a live imaging study of the sensory neurons innervating the pectoral fin skin. Sensory neurons in both the hindbrain and the spinal cord innervate the fin, with most of the population located in the hindbrain. The hindbrain somas are located in rhombomere 7/8, laterally and dorsally displaced from the pectoral fin motor pool. The spinal cord somas are located in the most anterior part of the cord, aligned with myomere four. Single cell reconstructions were used to map afferent processes and compare the distributions of processes to soma locations. Reconstructions indicate that this sensory system breaks from the canonical somatotopic organization of sensory systems by lacking a clear organization with reference to fin region. Arborizations from a single cell branch widely over the skin, innervating the axial skin, lateral fin surface, and medial fin surface. The extensive branching over the fin and the surrounding axial surface suggests that these fin sensory neurons report on general conditions of the fin area or a global stimulant (e.g. oxygen) rather than providing fine location specificity, as has been demonstrated in other vertebrate limbs. With neuron reconstructions that span the full primary afferent arborization from the soma to the peripheral cutaneous innervation, this neuroanatomical study describes a system of primary sensory neurons and lays the groundwork for future functional studies.

2.2 Contributions

In this chapter, I conducted the labeling experiments, imaged all the specimens, reconstructed all the neurons, ran the and clustering analysis. Alexander Roche calculated the morphological pa-

rameters for the neuronal reconstructions. Evdokia Menelaou helped conceive of the experiments and provided critical feedback in the progress of the chapter. The McLean Lab at Northwestern University contributed reagents and fish lines for this chapter. Drs. Sliman Bensmaia and Stefano Allesina assisted with identifying the appropriate statistical analyses. Haley Stinnett contributed her ingenious injection setup.

2.3 Introduction

The limbs of vertebrates are innervated with primary sensory afferents that provide input on both movement of the limb and properties of the animal's environment. In mammals, these sensory neurons are known to synapse directly with both local spinal motor neurons and ascending projection neurons relaying information to the brain [10, 159, 43, 1]. Like the skin of terrestrial mammalian limbs, the skin of aquatic vertebrate fins is also densely innervated by sensors [58, 123, 141, 25]. Fin sensory neurons transmit mechanosensory and other inputs from the fin [85, 12, 122, 135, 151], and that input modulates movement [150, 2]. To interpret fin mechanosensory physiology and function in behavior, a more detailed understanding of sensory neuroanatomy is required.

The larval zebrafish pectoral fin provides a complementary system to adult fish and tetrapods for examining vertebrate limb sensation. At 5 days post fertilization (dpf), the pectoral fins are flexible structures that are active during locomotor bouts and periodically when the fish is stationary [142, 41]. At this late larval stage, the fin can be subdivided into two regions: the fin body and the fin membrane. The fin body (FB) includes an endochondral disk separating the fan-shaped adductor and abductor muscle on either side [143]. Parallel to the endochondral disk, a simple set of muscles originate in the fin base and insert into the actinotrichia in the more peripheral fin membrane (FM), which eventually gives rise to the adult fin rays [143]. A single blood vessel bounds the FB from the FM. Movement studies have shown that the fin has a distinct curvature at this blood vessel during fin abduction [41, 40]. This articulation appears functionally analogous to the elbow joint of a tetrapod limb that allows bending in one direction.

The fins can beat rhythmically and have been shown to play a critical role in fluid mixing that occurs near the head and anterior trunk, thus supporting cutaneous respiration [41, 40]. Movement of the fin with the pair of muscles at the FB is coordinated by a pool of pectoral fin motor neurons that innervate the FB [142, 144]. This motor population has mixed origins in both the spinal cord and the hindbrain, consistent with myomeres two through five [97, 86]. Adductor and abductor motor neurons present a mixed mediolateral distribution within the pectoral fin pool [144]. These motor neurons give rise to the rhythmic asynchronous fin beats that encourage the mixing of the water immediately surrounding the fish. While prior work has indicated a sensory population innervating the fin [144], there has not been an in depth exploration of the corresponding sensory neurons.

For limb sensation in larval zebrafish and aquatic tetrapods, the focus of research has been on spinal cord sensory neurons; in larval zebrafish these are called Rohon-Beard cells (RBs). Early research in *Xenopus laevis* characterized RBs as transient mechanosensory neurons that innervate the body axis and respond to touch [124, 15, 16, 17, 58, 123, 141, 25]. These studies described RBs dying off during mid-larval stages [58, 120]. More recent work in zebrafish has found that RBs are not only intact at late larval to juvenile stages [104], they are also functioning as key touch responsive neurons in that species [29, 67]. At 5dpf, RBs have established connections with motor circuits [22, 57, 145, 71, 83]. As a functional sensory population at 5dpf, we hypothesized RBs would be innervating the pectoral fins.

We present here the first in depth description of the afferent arborization of the whole larval zebrafish pectoral fin surface. Using the larval zebrafish model, we aimed to determine how sensory neurons innervating the skin of the pectoral fin are organized as a population in the central nervous system (CNS). The robust genetic toolkit available in the zebrafish [8] facilitates the neuroanatomy work presented here. In addition, 5dpf zebrafish are small and transparent, thus allowing for *in vivo* approaches to study neuroanatomy. Here, we image the entire sensory innervation of the pectoral fin from CNS to peripheral skin. This *in vivo* preparation avoids distortion related to fixation and sample processing. Furthermore, we sought to assess afferent

anatomy and how it relates to other aspects of fin anatomy, movement, and function.

In exploring the cutaneous innervation of the 5dpf larval zebrafish fin, we sought to answer several central questions. First, what is the population identity of the fin sensory neurons (FSNs)? Based on prior work in the zebrafish motor system [86], we hypothesized that we would see a mixed population of hindbrain and spinal cord sensory neurons innervating the fin. Second, do the FSNs "map" to specific areas of the fin? Based on prior work in sea robin [94, 31] showing somatotopic organization of sensory innervation of the free fin rays, we anticipated that we would see some degree of somatotopy with FSN somas in the CNS organized according to their afferent patterns in the pectoral fins. Specifically, we expected more posterior somas to innervate more ventral regions of the fin. Based on prior data in axial RBs in zebrafish and *Xenopus laevis* [123], we also anticipated a high degree of branching of each primary afferent of each cell. Finally, we asked: is the innervation of the pectoral fin concentrated at the location of increased bending on the fin that occurs between the FB and the FM [41, 40]? Given the functional importance of this region, we expected some heterogeneity with greater innervation in the FM compared to the FB. In addition to describing sensory innervation, together with existing work on the motor system, these data support future studies exploring sensorimotor integration and fin function.

2.4 Materials and Methods

2.4.1 Fish

Animal use was approved by the University of Chicago's Institutional Animal Care and Use Committee. Adult zebrafish were maintained at 27°C on a 14/10 hour light/dark cycle in a custom fish facility. Fertilized eggs were held in 10% Hank's Solution in a 28.5°C incubator until 5dpf. At 5dpf, larval zebrafish were used for imaging studies and then euthanized in 0.02% 3-aminobenzoic acid ethyl ester (MS222, Sigma-Aldrich, St. Louis, MO, USA). To target sensory neurons, we used two transgenic lines that drive reporter expression in *islet2B*+ neurons [111, 102]. For initial studies examining the whole population, we used the *Tg[isl2b:GFP]*^{zc7} transgenic line

(*Tg[islet2b:GFP]*) [111]. In some cases, we used double transgenics by crossing *Tg[islet2b:GFP]* fish with *Tg[mnx1:Gal4;UAS:pTagRFP]* [160, 18] fish to examine the motor pool innervating the fin (Ma et al., 2010). We subsequently used *Tg[islet2b:Gal4]^{zc60}* transgenic animals (gift from McLean Lab, Northwestern University, Evanston, IL, USA; [19]) to achieve sparse stochastic labeling [8, 90], enabling the reconstruction of individual neurons.

2.4.2 Mauthner cell labeling

Tg[islet2b:GFP] fish at 4dpf were briefly anesthetized in 0.02% MS222 in Hanks. Once fish were non-responsive to touch, we placed them on a petri dish filled with 2% agar. Using 10% dextran conjugated with Alexa Fluor 647 (10,000MW Thermo Fisher Scientific, St. Louis, MO, USA), we followed the backfilling procedure described previously [45]. In these experiments, the capillary tube was aligned to be parallel with the ventral boundary of the spinal cord of the 4dpf larval zebrafish. Fish were allowed to recover post injections for 24 hours so that the dextran could thoroughly diffuse through backfilled neurons. Fish were then imaged on a Zeiss LSM 710 confocal microscope with a 20x dry 0.8NA objective.

2.4.3 UAS construct injections

Embryos from *Tg[islet2b:Gal4]* transgenic fish were collected immediately following fertilization. These embryos were then transferred to an injection plate composed of a plastic dish with a microscopy slide taped to it. Using capillary action with a Kimwipe (Thermo Fisher Scientific, Waltham, MA, USA) on the opposite side, embryos were aligned against the slide. In this arrangement, embryos at the one or two-cell stage were held stationary for DNA construct injections to generate stochastic labeling in the *Tg[islet2b:Gal4]* line with UAS:ptagRFP as described previously (gift from McLean Lab, Northwestern University, Evanston, IL, USA; [160, 90]). Following injections, embryos were transferred to fresh 10% Hanks and maintained at 28.5řC in a Fisher Scientific Low Temperature Incubator (Thermo Fisher Scientific, Waltham, MA, USA). After hatching at 3dpf, embryos were transferred to fresh Hanks and screened for single cell or sparse multi-

cell labeling in the pectoral fin using a Leica MZFLIII dissecting scope (Leica Microsystems, Inc., Buffalo Grove, IL, USA) with a mercury lamp as the excitation source.

2.4.4 Imaging

Fish were transferred to a 24-well plate to track left or right pectoral fin innervation. At 5dpf, fish were anesthetized in 0.02% MS222 in Hanks, and mounted laterally in low-melt agarose as previously described [45]. In this study, we used a round 35mm dish with high precision No. 1.5 coverglass (MatTek Corporation, Ashland, MA, USA) for optimal signal. To facilitate imaging of processes in the area of the yolk sac, the air bubble from the swim bladder was carefully removed with a patch pipette secured to a 1mL syringe with Parafilm. With this process, it was possible to remove the swim bladder from the non-imaging side of the fish with minimal disruption to the cells of interest. Embedded fish were imaged on a Leica TCS SP8 II STED laser scanning confocal microscope (Leica Microsystems, Inc., Buffalo Grove, IL, USA) under Köhler illumination conditions. We used the White Light Laser set to 555nm as the excitation source, and the specimen was imaged through a 40x/1.30 NA oil immersion HC PlanApo objective. For RFP, the detector was a HyD tuned to 562nm to 700nm with gain set to 20 and gating turned on, and for visible light the detector was a PMT with gain set at 415. We used bidirectional scanning with phase adjusted at the beginning of each imaging session. Pinhole was set for 1 airy unit. For each fish, we imaged a 3x3 region with excitation gain turned on through a 150 to 250 micron z-stack for a total of nine stitched images of 1024x1024 pixels at 8-bit depth using LAS X software (Leica Microsystems, Inc., Buffalo Grove, IL, USA), stitched in the software with statistical blending between tiles, and saved as .lif files.

2.4.5 Soma data

To calculate the size of single RB somas, we used the Bio-Formats [82] importer in Fiji version $2.0.0-rc-71/1.52p$, Java version $1.8.0_172$ [130, 131] to open .lif z-stack files for image processing on a desktop computer with an Intel Zeon CPU E5-2630 v4 @ 2.20GHz x 10, 62.8GiB of memory,

2TB hard drive, and an NVIDIA Corporation GM107GL [Quadro K2200] graphics card (Dell Round Rock, TX, USA) running Linux Mint 18.3 Cinnamon 64-bit (Cinnamon version 3.6.7, Linux Kernel: 4.10.0-38-generic, everyone, everywhere). In the full z-stack, we selected the single micron optical section in the middle of the soma along the medial to lateral axis. Using the freehand selection tool in Fiji, we traced around the fluorescent boundary of the cell body and recorded the value.

2.4.6 Innervation reconstruction

Whole z-stack tile scans were processed in Fiji [130, 131] using the Tubeness plugin [129] with a sigma value of 1. Output images were saved as 32-bit depth .tif files. We note that these files require substantial memory to open and work with. Post preprocessing for "tubes," we reconstructed the fin innervation of 21 RBs using the semi-automated Simple Neurite Tracer (SNT, version 3.1.3, [84]). Due to overlapping processes, we were able to accurately reconstruct the axial portion of only 12 neurons of the original 21 RBs. We reconstructed the fin innervation projections for 20 neurons. Fin afferent reconstruction was not performed on one RB since it did not branch in the fin. For detailed analyses of reconstructions, SNT .traces files were converted to .swc files and analyzed with a custom C script on a MacBook Air with macOS High Sierra 10.13.6 (Apple, Cuptertino, CA, USA). Traces were re-segmented to isolate the interbranch segments of each primary afferent. We selected a number of parameters utilized by NeuroMorpho.org [9], quantified the following metrics for each neuron: 1) number of branch points, which is the total number of branches of the afferent in the fin and the processes leading up to the fin (if the processes branch before the fin), 2) maximum order of any branch on the tree, which is how many branch points (n) are between the soma and the end point of the most branched afferent (n + 1), 3) Strahler number, which is the degree of branching as calculated backwards from each terminal branch as 1, subsequent more basal branches are n + 1 if both daughters are n, alternatively the next branch is also n if one daughter is n and the other is less than n, 4) average partition asymmetry over all of the branch points, which is the measure of asymmetry of the tree where 0 is completely symmetric and 1 is highly asymmetric, 5) maximum path distance from the soma

to any terminal point, the longest afferent from the soma to the terminal point, 6) the average contraction of the neuron, the ratio of the euclidean distance of a path to the actual path length that generates one estimation of the space filling of a neuron, 7) the average angle of the branches near the branch point, which is the Euclidean distance of each segment divided by the total length of the neuron, 8) the average local angle, which is the immediate angle 10 nodes (pixels) away from the branch point in each segment, 9) the average remote angle, which is the angle 10 nodes (pixels) away on the next daughter branch, 10) the average fractal dimension of the branches, which is a measure of how much the afferent meanders with a straight line being one and a more meandering line having a slightly higher value than one, 11) total length of all segments, all of the lengths of the segments projecting to the fin added together from the initial branch off the soma to the entire innervation of the fin, 12) the area of the soma, which is calculated at a single micron z-slice from the confocal z-stack 13) the position of the soma, which is calculated with reference to the boundary between myomeres three and four [9].

2.4.7 Neuronal classification

Based on the number of FSN RBs in the dataset, we opted to use a hierarchical clustering algorithm to examine the dissimilarities among the 20 reconstructed neurons that exhibited branching in the fin. Data were scaled in R (R version 3.6.3 (R Core Team, 2014), RStudio Version 1.2.5042 ([127]) such that the mean over all neurons was 0 and the standard deviation was 1. A dissimilarity matrix based on the Euclidean distance of the individual measures of each of the 13 parameters was established. We used agglomerative hierarchical clustering using Ward's linkage method [30] in R. In this method, individual neurons, the leaves, are iteratively combined into nodes based on the similarity between them. Grouping continues until all the leaves are part of one big cluster. We used the average silhouette method to confirm the optimal number of clusters. This method allows for intracluster evaluation of similarity, which is how well an individual fits within its cluster.

2.4.8 *Quantification of axis and fin innervation overlap*

Even with sparse stochastic labeling, there was overlap of primary afferent arborizations on the axis that made it difficult to reconstruct individual neurons. Due to this overlap, we were restricted to full reconstructions of fin and axis innervation in only 12 neurons. All of them had their cell bodies in the hindbrain. When the fin is adducted it lies close to or against the axis. To examine the spatial relationship of the axial innervation relative to the fin innervation of a cell we examined how axial innervation and fin innervation overlap, and potentially interact, in this region. We designated a "model fin" that was used as a stereotyped fin across those sampled. This model fin was an average of all the fin contours collected. A 2D projection of the model to its best-fit plane was rotated and moved for each fish such that the midpoint of its base and the angle its base made with the body matched up to the actual fish's fin. The axial innervation was projected onto the plane defined by this fin, and innervation within this area was assumed to be contacted by the fin during adduction. The total length of the innervation within this area, along with the percentage of the total axial innervation within this area, was calculated for each fish.

2.4.9 *Fin quadrant innervation*

To analyze the innervation patterns within the fin, we divided the fin into eight regions. Lateral and medial surfaces were both examined. For each, the FM and FB were bisected into ventral and dorsal portions (see 2.5 A), generating a dorsal and ventral FM region and a dorsal and ventral FB region for both the lateral and medial surfaces. We used the Bio-Formats importer [82] in Fiji [130, 131] to open the fluorescent and brightfield confocal z-stacks. We merged the two images together and used the multipoint function in Fiji to assign 18 points in three-dimensional space: nine points on the outer edge of the FB as demarcated by the blood vessel and nine points on the edge of the FM. Of each of these sets of nine points, two points were at the base, one on either side, one point was at the maximum distance from the base, and, on each side of that point, there were three points that roughly defined the shape of the fin. In Mathematica version 12.0.0.0 (Wolfram Research, Champaign, IL, USA), we used the 14 non-base points to find a best-

fit plane onto which we orthogonally projected all of the points. We also projected each of the 21 reconstructed neurons onto this plane, one at a time. We divided the plane into quadrants based on the fin points: the dorsal and ventral portions of FB and FM. A line from the midpoint of the proximal and distal points of the fin body to the median point on the fin membrane defined the dorsal/ventral boundary (Fig. 2.5 A). In SNT, we tagged the primary afferents to segregate them into medial surface innervation and lateral surface innervation. Altogether, we had eight different possible fin locations. In Mathematica, we calculated the total length of each primary afferent in each of these octants.

2.4.10 Figure preparation

We generated a duplicate set of microscopy images specifically for image preparation. Stitched, tiled z-stacks were projected along the z-axis, smoothed in Fiji, and flattened. We generated merged two channel images as well as z depth color coded single channel images. When necessary, we cropped processed images for specific regions of interest. All graphs were generated in RStudio using ggplot2 [148]. All figures were arranged in Adobe Illustrator (Adobe, San Jose, CA, USA).

2.5 Results

2.5.1 Pectoral fin surfaces are innervated by projections of neurons from the hindbrain and spinal cord

Sensory neurons labeled in *Tg[islet2b:GFP]* transgenic fish have somas in the hindbrain and spinal cord, and their processes can be seen innervating the pectoral fin (Fig. 2.1 brightfield compared to Fig. 2.1 fluorescent images). This transgenic line, labeling the entire population of sensory neurons, was used to examine the broader features and locations of the somas of fin-innervating cells. We used the *Tg[islet2b:GFP]* x *Tg[mnx1:Gal4;UAS:pTagRFP]* double transgenic fish to examine the sensory neuron cell bodies relative to motor pools in the CNS (Fig. 2.1). There are two

distinct populations of motor neurons visible in the z-projected z-stack: a spinal population and a hindbrain population (Fig. 2.1) shown previously [86]. The spinal cord motor neuron population

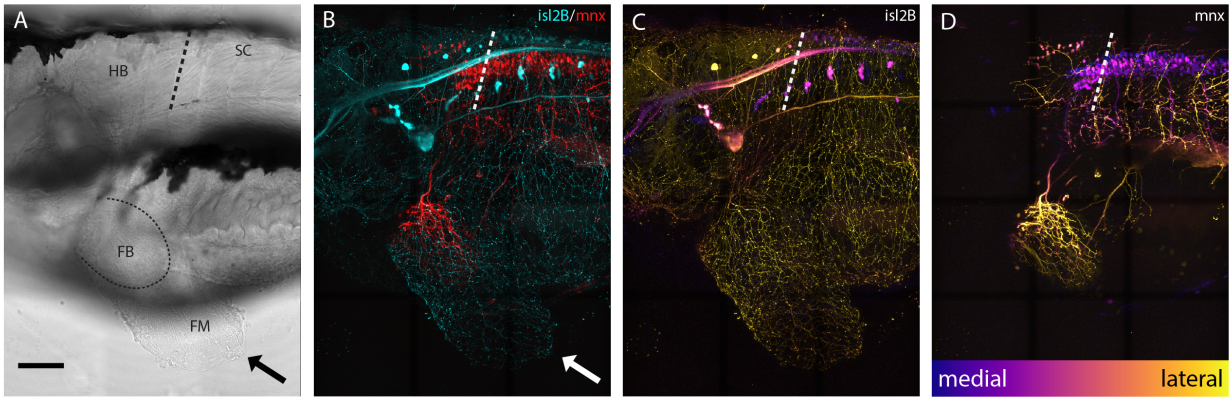

Figure 2.1: *islet2B+* neurons innervate the pectoral fins of 5dpf larval zebrafish. (A) Brightfield lateral view of a 5dpf larval zebrafish. Arrow indicates distal fin membrane, and dotted line indicates the blood vessel boundary between the fin body (FB) and fin membrane (FM). (B) *Tg[islet2B:GFP]* x *Tg[mnx1:tagRFP]* double transgenic fish (N = 4) showing sensory neurons and their processes (cyan) and motor neurons and their processes (red). Arrow indicates distal fin membrane. (C) Depth coded z-projection of islet2B+ neurons highlights the lateral placement of the sensory neuron cell bodies compared to the more medially located mnx1+ motor neurons in panel D. Depth scale is the same for (C) and (D). Anterior is to the left, dorsal is up in all images. Scale is 100 microns.

appears larger than the hindbrain motor neuron population (Fig. 2.1). We find that the FSNs are distributed similarly with both a hindbrain and spinal cord population. The hindbrain FSNs are located more lateral and dorsal with respect to the motor neuron population (Fig. 2.1). In the spinal cord, GFP+ Rohon-Beard neurons (RBs) (Fig. 2.2, n = 4), are located at the dorsal margin of the cord, and their processes innervating the fins extended from the RB pool associated with myomere four and five. The total number of RB somas associated with myomeres four and five ranged from six to eight (n = 4).

The hindbrain component of the FSN pool was anterior to the boundary between muscle myomeres three and four (orange line, Fig. 2.2) and located in hindbrain rhombomere 7/8. In the hindbrain FSN population, a minimum of two cell bodies (not shown) and a maximum of seven cell bodies were labeled per fish (Fig. 2.2) (n = 14 fish). To refine information regarding the location of the hindbrain fin sensory neurons, they were examined in *Tg[islet2b:GFP]* fish that

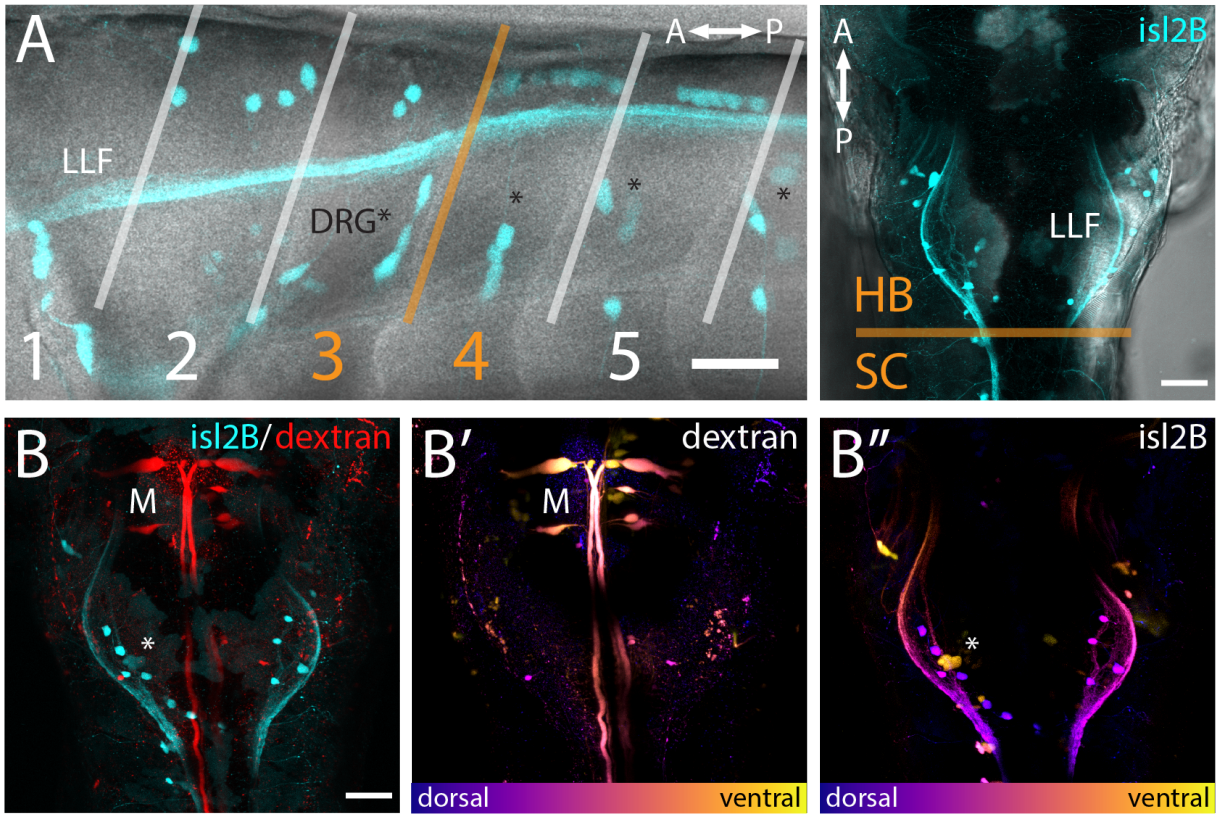

Figure 2.2: FSNs have somas in the hindbrain and spinal cord. (A) Left panel: Brightfield and fluorescent merged image adjacent to myomeres one through five, indicating the distribution of the *islet2B*+ somas (cyan) innervating the fin. The somas innervating the fin are located dorsal to the dorsal root ganglia (DRG neuron) neurons visible as clusters (asterisks). The lateral longitudinal lateral longitudinal fasciculus (LLF) extends from the hindbrain into the spinal cord. The transition area between myomeres three and four, historically referred to as the transition between the hindbrain and spinal cord, is indicated in orange. Cells posterior to the boundary are located in the spinal cord, and islet2B+ cells in this location are Rohon-Beards. Right panel: Brightfield and fluorescent merged image of a dorsal view of a *Tg[islet2B:GFP]* fish. The hindbrain and spinal cord boundary is again marked in orange. The organization of the sensory neurons along the lateral margins of rhombomere 7/8 is bounded by the LLF. (B) All of the somas (cyan, left panel) are located posterior to the Mauthner neurons (red, M). Additionally, Mauthner neurons are notably more ventral (M) in the hindbrain than the FSNs (asterisk is DRG neuron). Anterior is to the left, dorsal is up in (A left panel). Anterior is up, dorsal view in (A right panel and B). Scale is 40 microns in (A left panel) and 50 microns in (A right panel and B).

had been secondarily labeled through injection of dextran to fill reticulospinal cells (Fig. 2.2) (n = 10). The most anterior *islet2B+* neuron in each fish was on average 184.38 $\pm$8.83μm (average $\pm$ SE) posterior to the Mauthner neurons, which are located in rhombomere 4 [69]. Mauthner neurons are on average 279.82 $\pm$7.93μm from the HB/SC boundary, as previously defined [93, 87, 86], confirming that these fin neurons are well within the hindbrain. In lateral view (Fig. 2.2), FSNs show a range of dorsoventral positions. In dorsal view, labeling of the lateral longitudinal fasciculus (LLF), provides a marker along the mediolateral axis (Fig. 2.2 A, right). The fin sensory neurons that we observed were all located medial and dorsal to the LLF and dorsal to the level of Mauthner neurons (Fig. 2.2 B).

2.5.2 Fin sensory neurons show a variety of soma morphologies

We analyzed individual neurons in 21 sparsely labeled *Tg[islet2b:Gal4]* larval fish injected with UAS:ptagRFP, again using confocal microscopy. In these stochastic labeling experiments, a large majority of the cells (17 out of 21) were located in the hindbrain. The remaining cells were RB neurons in the spinal cord, of which three were associated with myomere four and only one was associated with myomere 5. The population of FSNs sampled exhibited a range of morphologies. At the level of myomere two, a total of three neurons were labeled. One of the cells was circular and 178.60μm^2, another was asymmetric, spherical, and 105.03μm^2, and the third was teardrop shaped and smaller at 92.24 μm^2 (2.3, A, clockwise second image). In myomere three, where 14 cells were labeled, we observed seven spherical cells ranging from 61.39μm^2 to 117.31μm^2, four teardrop shaped cells ranging from 48.9μm^2 to 88.95μm^2, and three inverted teardrop shaped cells that were 73.82μm^2, 79.44μm^2, and 85.64μm^2 (2.3 A, clockwise third image). In contrast, all of the spinal neurons at the levels of myomeres four and five (n = 4) exhibited the classic morphology of RBs: they were elongated along the anteroposterior axis, dorsally displaced, and arranged in a columnar fashion in the dorsal most regions of the spinal cord (2.3 A, clockwise fourth image). RBs ranged from 84.56 to 107.56μm^2 in cell area (mean 93.77μm^2, SD = 9.76μm^2, Fig. 2.3). There is no significant difference in the areas of HB FSNs and RB FSNs (Fig. 2.3 B, ANOVA, $p > 0.05$).

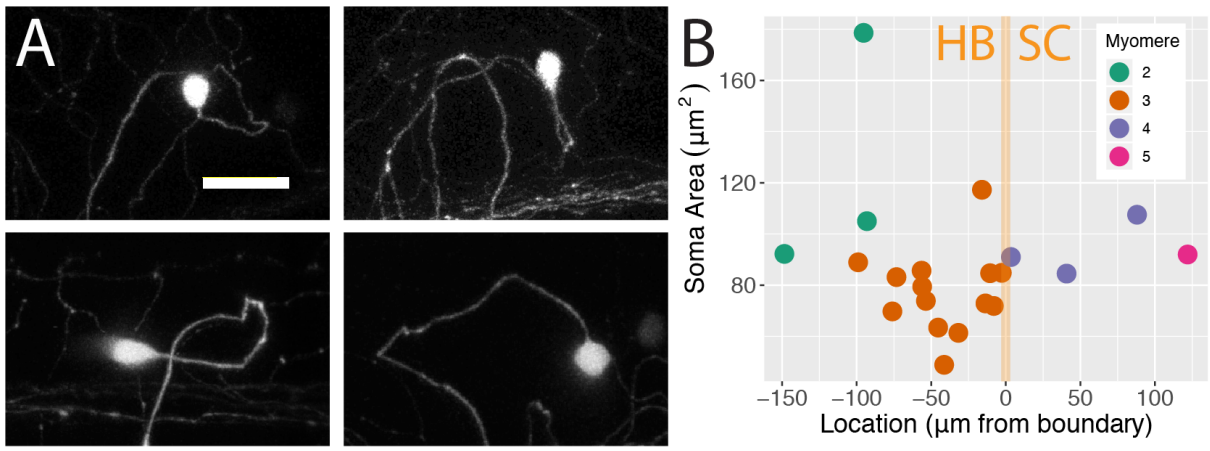

Figure 2.3: FSNs exhibit a variety of soma morphologies. (A) The four main FSN soma morphologies clockwise from top left: small spherical hindbrain (HB), small teardrop HB, rounded HB with dorsal projection, and a classic RB elongated along the anteroposterior axis. The three hindbrain morphologies are apparent across cells associated with myomeres two and three. (B) FSNs are distributed across myomeres two through five, and they show no significant trends in soma size or distribution patterns across the anterior to posterior axis within any of these myomeres. FSNs exhibit no trends with regard to the hindbrain/spinal cord transition area (indicated in orange). Negative numbers are consistent with a hindbrain location, and positive numbers indicate a spinal cord location. Most of the cells innervating the fin are found in myomere three. (D) Anterior is to the left, dorsal is up in (A). Scale is 25μm in (A).

2.5.3 FSNs innervate the axis and extend concomitant projections to the fin

FSNs projected towards the fin in two different manners. At this stage in development (5dpf), the pectoral fins are comprised of fan-shaped musculature in the fin body (FB) and a surrounding thin cutaneous fin membrane (FM) (Fig. 2.4). The processes of the FSNs exit the CNS and establish extensive innervation projections along the axis and into the fin (Fig. 2.4). All 21 of these neurons showed extensive innervation across the skin of the axis. At the level of the skin, FSN processes track to the fin body and enter the fin in two possible configurations. In five out of 21 cases, FSNs had two branches that eventually projected into the fin (Fig. 2.4) whereas the majority of the reconstructed neurons (16 out of 21) had a prominent process that projected to the fin with no secondary projections that concomitantly entered the fin (Fig. 2.4). Once the FSNs innervated the fin, they tended to project to fill the entire fin on both the medial and lateral sides. In preliminary examination, 19 of the 21 neurons had initial projections onto the medial surface

of the fin only while 16 of the 21 neurons had initial projections onto the lateral surface of the fin only. In the majority of neurons examined, the individual neurons innervated both sides of the fin. Afferents of many neurons wrapped around the fin membrane to innervate the opposite side. In two cases, reconstructed neurons innervated the fin, looped around and exited the fin. While the processes crossed over the surface area of the muscle in the FB, we never observed stochastically labeled cells with fiber endings in the FB muscle. The primary afferents exhibited occasional varicosities along their superficial primary afferents, but they lacked any obvious associated sensory structures, ultimately terminating in free nerve endings.

2.5.4 FSNs form three clusters based on morphological parameters

We deconstructed the primary afferent reconstructions into individual branch components and analyzed 11 tree morphological parameters and two soma parameters. With these 13 parameters, we explored potential subtype classifications among the 20 individually reconstructed neurons with hierarchical clustering analysis (Fig. 2.4). As stated previously, the 21st neuron was eliminated due to its lack of any branches in the fin. Three clusters of neurons emerged: one group of highly arborized fin specific processes, a second group with less dense branching, and a third group containing a single neuron that has very limited branching in the fin. The first group contains 14 neurons that are spread across four arbitrary units (purple, Fig. 2.4). This group has a variety of neuronal morphologies represented (Fig.2.4), with some cells exhibiting distally biased process branching (cell 2 in purple cluster one) and others exhibiting more even branching (cell 20 in purple). The second group contains five closely related cells (green, Fig. 2.4). In contrast to the first cluster, this second cluster (cells 6, 10, 14, 9, and 15 in green cluster two) exhibits higher degrees of branching and larger innervation lengths (Fig. 2.4). The third group, with just a single cell, is noticeably disparate from either cluster (Fig. 2.4, cell 11 in yellow cluster three). Notably, HB and RB FSNs are intermixed in these two clusters. The cluster arrangements remained when individual morphological components were removed and the clustering analysis was re-examined (e.g. removal of Strahler number values had minor effects on the cluster organization).

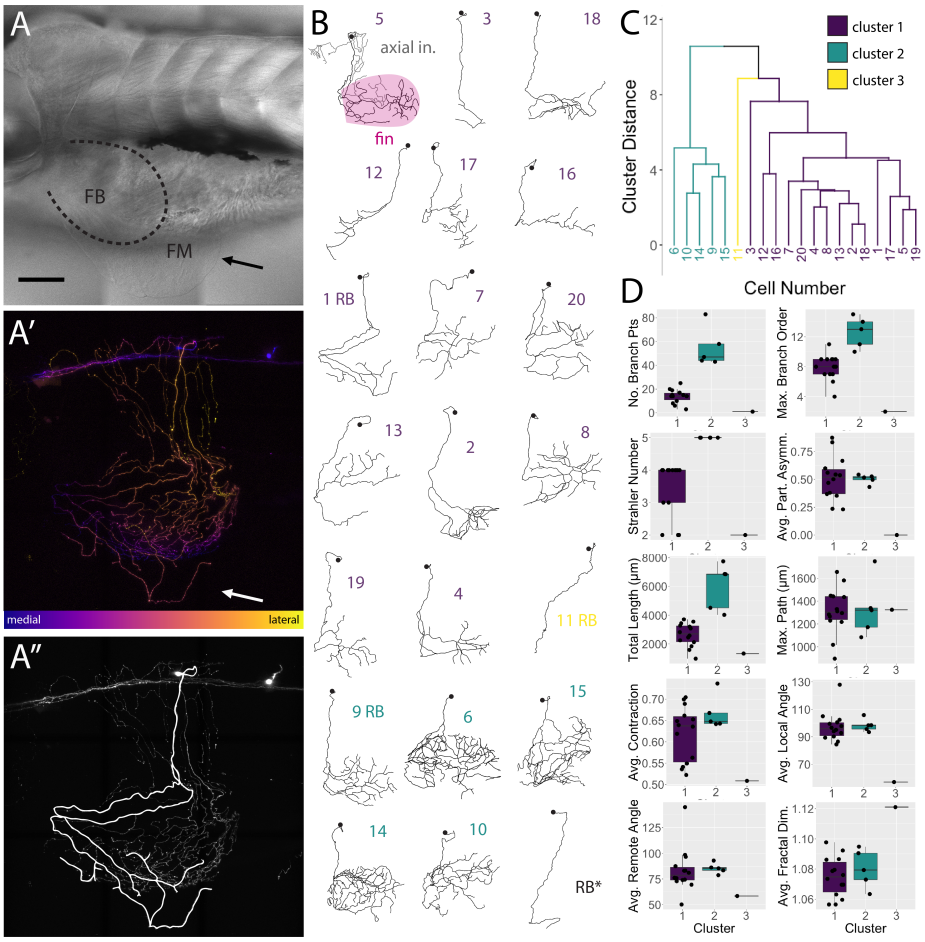

Figure 2.4: *islet2B+* neurons innervating the fin fall into three distinct morphological clusters. (A) Brightfield image of 5dpf larval zebrafish in lateral view. The fin is indicated with a black arrow, and the fin body (FB) is bounded by a dotted line indicating the position of the blood vessel separating the FB and the fin membrane (FM). (A') A depth coded z-projection of a single *islet2B+* neuron from the same fish in (A) shows an extensive arborization on the body and some sparse processes visible in the fin (white arrow). (A") The same z-projection with an overlay of the reconstruction of the primary afferents projecting into the fin. (B) Reconstructions of the primary afferents innervating the fin show a diversity in both innervation pattern and fin coverage. The reconstruction in the top left has the axial innervation included in gray, the rest of the reconstructions are of only the fin innervation. The numbers are color coded to correspond to one of the three clusters in (C). The last reconstruction innervated the pectoral fin with a single unbranched process, and this one was excluded from the clustering analysis due to its unbranched nature (RB*, black). (C) Dendrogram of the results of agglomerative hierarchical clustering analysis using Ward's method. There are three distinct clusters, color coded to reflect the number labels associated with the neuronal reconstructions in (B). The y-axis indicates the Euclidean distance between clusters and leaves. (D) Box plots of each of the 10 morphological parameters, together with two soma parameters from Figure 3, utilized in the cluster analysis. Boxes are color coded in accordance with cluster number, with the exception of cluster 3, which only contains one cell. Black point overlays indicate the individual values for each neuron. Anterior is to the left, dorsal is up in (A, A', A"). Scale is 100 microns in (A). N = 21 in (B) and 20 in (C & D).

Morphological parameter results detailed in Table 2.1.

Morphological Parameter	Min Value	Max Value	Mean	Median	SD	Shapiro-Wilk Normality p-value
total length of innervation (μm)	971.92	7751.764	3409.5	3139.8	±1857.869	0.019
average contraction of the neuron (AU)	0.509	0.736	0.6252	0.642	±0.066	0.121
number of branch points (AU)	1	83	23.5	15	±20.92719	0.002
maximum path distance (μm)	896.526	1748.026	1319.7	1315.8	±202.6641	0.755
average branch fractal dimension (AU)	1.056	1.121	1.078	1.077	±0.016	0.303
average partition asymmetry (AU)	0	0.875	0.483	0.509	±0.198	0.371
average local angle (°)	57.0805	127.903	95.54	96.11	±12.807	0.005
average remote angle (°)	50.165	144.936	82.62	82.04	±18.692	0.003
maximum euclidean distance (μm)	349.222	699.373	491.2	467.3	±89.653	0.227
Strahler number (AU)	2	5	3.75	4	±1.070	0.002
maximum branch order (AU)	2	15	9	0	±3	0.612

Table 2.1: Numbers for all the morphological parameters used to investigate primary afferents in the fin. Shapiro-Wilk Normality p-value > 0.05 indicate data is normally distributed (n =20 fish).

2.5.5 Primary afferents are not "mapped" to FB or FM, but do "map" to the mediolateral surfaces

We hypothesized that, between the two main clusters of neurons, there may be distinct innervation patterns with reference to the pectoral fins themselves. Specifically, we sought to answer whether or not the FSNs exhibited any evidence of a fin "map," with specific projections to certain areas. FSNs of the two clusters innervated the pectoral fins in a seemingly random manner (ANOVA, $p > 0.05$). Given the organization of the FSN population across the hindbrain and the spinal cord, we next examined the anteroposterior organization of the peripheral processes with regards to the total length of fin innervation. More anteriorly located FSNs had higher total afferent lengths in the fin than their more posterior counterparts (ANOVA, $p = 0.04$, Fig. 2.5). Due to the longer initial axial segment leading to the fin projecting to the RBs, we re-examined these data without the RBs. This trend remains significant without the RBs (ANOVA, $p = 0.031$). Based on this trend in overall afferent length, we sought to examine any potential "map" arrangements in the fin. Here, we describe innervation patterns established along the dorsal and ventral part of the fin, pink for dorsal and green for ventral (Fig. 5A). We also delineate between the FB and the FM, light pink and dark pink, respectively. By rotating the reconstructions, we could further subdivide the quadrants into octants based on their positioning on the medial or lateral surface

of the fin (Fig. 2.5 right panel).

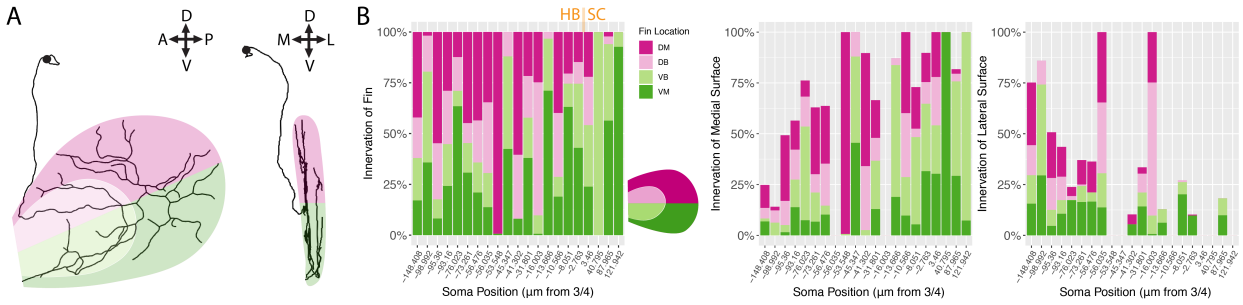

Figure 2.5: Fin sensory neurons exhibit biases to specific fin areas depending on soma location. (A) A single neuron reconstruction shows coverage of all four quadrants (left panel), and also shows bias towards the medial surface of the fin (right panel). Note: due to the nature of the projection in the right panel, the overlay of the dorsal and ventral shadings is consistent with the shading at the level of the blood vessel. (B) The distribution of primary processes across the fin quadrants including the dorsal membrane (DM, dark pink), dorsal base (DB, light pink), ventral base (VB, light green), and ventral membrane (VM, dark green). There is notably more innervation of the medial fin surface (middle panel) across all quadrants compared to the lateral fin (right panel).

In the four main quadrants (the ventral and dorsal FB and the ventral and dorsal FM), there was no clear preference for one section over the other (Fig. 2.4). Primary afferents did not preferentially innervate the FM, as hypothesized, and they did not preferentially innervate the FB in either the dorsal or ventral regions (ANOVA, $p > 0.05$, Fig. 2.4). There were two cells that had highly biased innervation patterns, one innervating almost exclusively the dorsal membrane and one innervating almost exclusively the ventral membrane (Fig. 2.4). In all the other cases, the distribution of the primary afferents across the fin quadrants lacked any clear organizational pattern. In no cases did we observe an obvious preference for the "joint" region that bends between the FB and the FM. As stated above, the logical next investigation was the examine the functional octants of the pectoral fin.

Despite the lack of notable organization with respect to the FB or the FM, or the "joint" formed between the two areas, there was a trend in innervation of the mediolateral surfaces of the fin. Most of the primary afferent innervation in the fin was on the medial surface of the fin (Fig. 2.4 middle panel). Correspondingly, the more posterior located FSNs innervated the lateral surface

less (ANOVA, $p < 0.01$). This relationship was maintained even when we removed RBs from the dataset. The mediolateral innervation bias reflects a broader trend that we examine further below.

2.5.6 Sensory neurons innervate the body wall as well as the fin

Regardless of their soma locations, all stochastically labeled cells examined innervated the skin of the body wall as well as the fin. In the interest of exploring the relationship between the fin surface and the axial surface, we reconstructed axial branches on 12 of the 21 FSNs that had no overlap from other stochastically labeled cells on the axial skin. The lack of overlap allowed unambiguous assignment of the processes to the FSN of interest. These 12 neurons exhibited innervation both posterior to and anterior to the base of the fin (Fig. 2.6). In many cases, we observed innervation on the axis under the fin (Fig. 2.6). The extent of axial innervation was comparable to that of the fin, with no significant difference between the total afferent length innervating the axial skin compared to the total afferent length innervating the pectoral fin surface (Fig. 2.6 B, right panel, Chi-square test, $p > 0.05$).

We examined the number of terminals on the medial and lateral surface of the fin as well as on the axis under the fin. As with the innervation percentages in the octants, we found a significant trend in mediolateral organization of terminals. We found that the number of medial surface fin terminals correlates positively with the number of terminals on the axial surface under the fin (correlation, $p < 0.01$) (Fig. 2.6 C, right panel left graph in purple). In contrast, no significant relationship was apparent between lateral surface fin terminal numbers and the number of terminals on the axial surface under the fin ($p > 0.05$) (Fig. 2.6 C, right panel right graph in orange).

2.6 Discussion

The small size and transparency of the larval zebrafish and the molecular tools available to interrogate neuronal morphology make it possible to take a whole-structure approach to understanding limb innervation in a vertebrate. Here, we describe the sensory innervation of the pectoral

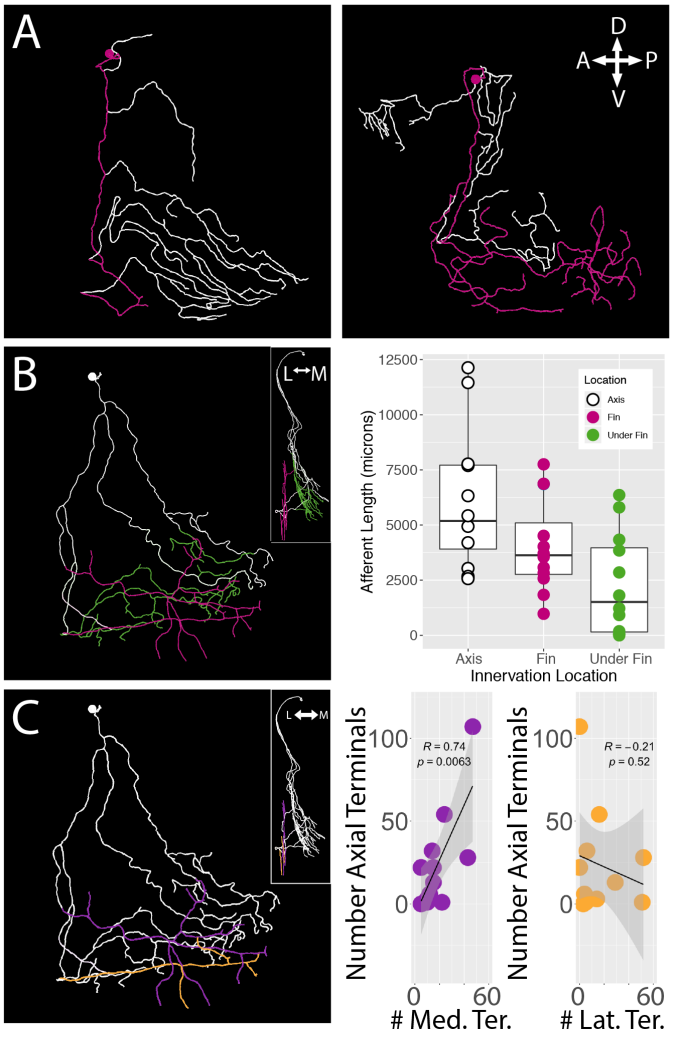

Figure 2.6: islet2B+ neurons innervate both the fin and the axis. A subset of single neuron reconstructions color coded to indicate the axial innervation in white and the fin only innervation in pink. (A) Left, the cell has very little fin innervation and the primary afferent that enters the fin loops back out of the fin. Right, the cell has far more extensive coverage of the fin. (B) Left, a third cell is color coded for axial innervation (white), fin innervation (pink), and axial innervation under the fin (green). The inset image shows a 90 degree rotation of the same fish with the same color coding. Right, there is a substantial amount of axial innervation across all sampled fish, and the amount of axial, fin, or under the fin innervation varies across a wide range of afferent lengths. In general, the whole population has higher primary afferent lengths on the axis compared to the fin. Notably, some fish have zero to very little innervation under the fin. (C) Left, the same reconstruction in (B) is color coded for medial fin innervation (purple) and lateral fin innervation (orange). The inset again shows the same reconstruction rotated 90 degrees. Right, the number of terminals on the medial fin surface is positively correlated with the number of terminals on the axial surface under the fin (purple graph, correlation, $p < 0.01$). The number of terminals on the lateral fin surface shows no trend in relation to the number of terminals on the axial surface under the fin (orange graph, correlation, $p > 0.05$). Anterior is to the left, dorsal is up in reconstructions. In insets, medial is to the left and dorsal is up.

fin, a vertebrate forelimb homolog. We show that the 5dpf larval zebrafish pectoral fin is innervated by both hindbrain and spinal cord FSNs. The morphology of the spinal cord neurons is consistent with that of RBs. The HB FSNs appear distinct from the classic RBs based on both their brain location and cell body morphology. Our finding of both hindbrain and spinal sensory innervation builds on prior work describing the somas of the pectoral fin motor pool in both the hindbrain and the spinal cord [87]. Prior work in the sea robin, *Prionotus carolinus*, showed that a functionally unique chemosensory system had nerves originating solely in the spinal cord from specialized accessory spinal lobes that are formed by fusion of the dorsal root ganglia with the dorsal horn [31, 135]. Our results highlight a mixed sensory neuron population, demonstrating more complexity in the organization of sensory fin neuron populations across fish species and/or life stages than previously recognized. The highly varied arborization patterns and the extensive innervation of both the fin and body wall suggest a lack of specificity for regions of the fin, thus raising questions regarding the function of the zebrafish FSNs. Future functional studies may be able to tease apart the relationship of our neuroanatomical findings to cellular function.

2.6.1 Functional implications of morphological features

The overwhelming majority of fin neurons labeled were located in rhombomere 7/8 (r7/8) of the hindbrain. We define r7/8 by its alignment with muscle myomeres one through three, and it is the most posterior of hindbrain rhombomeres. Accordingly, this region of the brain is in close proximity to spinal neurons [113, 138, 87, 24], but it is considered anatomically and functionally distinct. As zebrafish are Cypriniforms, an order of teleost fish possessing a unique vocal apparatus by adulthood, it is important to note that this hindbrain region is the location of inferior olive neurons, respiratory neurons, and vocal pacemaker neurons [14, 87, 13]. Throughout development, the region between myomeres one through six undergoes a number of developmental changes as the vocalization function appears behaviorally [93]. These features suggest a number of potential targets for hindbrain FSNs.

The variability in cell number observed in the hindbrain FSNs labeled in the *Tg[islet2b:GFP]*

is interesting with respect to canonical descriptions of other hindbrain neurons, like the reticulospinal neuron array, which is much more stereotypical in morphology and location of individual neurons [69]. It is possible that there is some variability innate to this particular transgenic line. As previously described in sensory neuron populations, different enhancers drive expression at different times and in the same population of cells [104]. Alternatively, there are some other potential factors that could be leading to the variable numbers. First, the 5dpf larval zebrafish is at the beginning of a transition stage in ontogeny during which the free-swimming larvae are beginning to hunt and feed. The larval fish pectoral fins are undergoing extensive growth and development [143], and, as a result, there is likely significant remodeling of the sensory system during this period. Second, at around 7dpf, larval zebrafish begin to transition from cutaneous respiration to gill based respiration. It is possible that, as the 5dpf larva progresses through the life history stages that require different sensory feedback and new motor repertoires, the sensory system must change to accommodate these needs. Additionally, perhaps variability in zebrafish neuron population numbers is not uncommon, as adult zebrafish exhibit widespread adult neurogenesis [163, 54]. On top of this, RBs have been described as a transient sensory neuron population that is lost during the larval stages as dorsal root ganglion neurons (DRG neurons) overtake some of their functions [153]. There is evidence that numbers of neurons are variable in a variety of organisms [72, 88, 73] review in [152]. In addition, adult neurogenesis in zebrafish results in about 6000 new neurons in the brain every 20 minutes [54]. If the FSNs are in a similar period of transition, then it logically follows that we would observe variable numbers of FSNs reflecting the changing life history demands. Perhaps during this phase of rapid and extensive remodeling, the FSN population is undergoing equivalent changes. Furthermore, dorsal root ganglia neurons innervate the pectoral fin beginning at this stage (data not shown). This developmental timing, while not functionally linked to the turn over of RBs [149], may indicate a transitional period in the sensory architecture of the pectoral fin.

We found that fin sensory neurons of larval zebrafish also innervated the body wall adjacent to the fin. The number of terminal branches on the medial fin surface is positively correlated with

the number of terminal branches on the body wall. In this context, our results suggest that, while somatotopic organization of fin sensory systems is apparent only at later stages in DRG neurons, trends in mediolateral terminal distributions may already be in place at larval stages. Future studies could further explore these trends across ontogeny, and functional studies could unravel the physiological importance of the mediolateral bias. Or, more simply, perhaps this organization is an early transition stage building the framework for a later anteroposterior organization. Prior work has examined the anteroposterior organization of fin nerves innervating both the larval and the adult zebrafish fin [144]. In other specialized fish species, such as the sea robin [31] there is a similar organization. Importantly, these later stage fin nerve descriptions are most likely from DRG neurons. Perhaps trends in mediolateral terminal distributions are early drivers or landmarks for later developing sensory neurons that exhibit somatotopic organization along the anteroposterior axis.

That the FSNs of larval zebrafish innervate the skin of both the pectoral fins and the body axis suggests that they are not well suited for proprioception in the fin, as has been proposed for fin sensation in mature fish [151]. If the FSNs are mechanosensitive, they would be activating their own processes both in the fin and under the fin. Instead, it appears that these FSNs are likely to be nonspecifically detecting stimuli across a large area of the larval body and pectoral fin. In this context, it seems unlikely that the FSNs would be activated by somatosensory stimuli specific for the fin itself. If they were, these cells would presumably be activated constantly as the fins are actuated. Instead, we propose that these limb sensors may be involved in chemosensory function related to cutaneous respiration, or they may be functioning as general rhythm detectors. Prior work has established r8 as the location of rhythmic motor neurons [14, 87], and the role of rhythmic pectoral fin movements in fluid mixing has been established [41, 40]. A sensory population in this region would provide feedback on the nature of rhythmic systems critical for cutaneous respiration. Future functional studies could investigate these hypotheses in order to untangle the functional role of the FSNs.

Functional investigation would be particularly insightful within the fin. At later stages of

ontogeny, the FM will eventually give rise to the fin rays [39], which we know from prior work encode proprioceptive feedback on fin ray bending in a number of species [151, 3, 47]. In some cases, fin rays have also been shown to provide chemosensory feedback [31, 135] and this is also likely to be more common than previously appreciated [46]. Subtypes in trigeminal neurons have been described at the morphological level [105], and *trpa1b* has been identified as an important channel in RBs regulating the response to nociceptive chemical stimuli [114, 33]. Taken together, we propose that the FSNs of larval zebrafish are involved in different sensory processes beyond mechanosensation, the known feature of RBs.

2.6.2 Sensorimotor remodeling across ontogeny and the fin to limb transition

Prior work has shown that RBs are a transient population that begins to die off at some point during late larval stages. Initial reports suggested RB cell death began around 5-7dpf [149]. However, several more recent studies have found that at least a subset of RBs are present at later stages, at least until 16dpf [104]. In our lab, RBs have been anecdotally observed until at least 14dpf. Thus, the FSNs in both the hindbrain and spinal cord are possibly intact throughout the larval ontogenic changes to the fin. It will be necessary in future studies to explicitly identify the fate of these cells through ontogeny. If they are a transient population like RBs, there will be a need to determine when they die off and what sensory population replaces them.

Honing in on the functional and morphological changes during ontogeny could shed light on the structural and functional changes of sensory systems across evolution. Teleost fish have developed a number of ways to repurpose paired fins for specific environmental needs [31, 135, 96, 4, 78], and there is plentiful evidence for variance in brain organization and structure across evolution [126, 95]. Prior work in evolutionary developmental biology has indicated that the shift of pectoral fin motor neurons from a mixed hindbrain and spinal cord population to only a spinal cord population, as found in forelimb motor neurons in mammals, has largely happened as a result of a shift in Hox gene expression [113, 138, 87, 24]. We have found that the sensory system in larval zebrafish follows the same pattern as the motor system, and the genetic patterning respon-

sible for this will be interesting to investigate. A full description of the sensorimotor patterning in the zebrafish, together with the plentiful genetic tools available, could provide a playground within which to explore how the sensorimotor system of paired appendages can be remodeled.

Interestingly, this is the first time that sensory neurons from the hindbrain have been described as innervating paired forelimb appendages. The sensory neuron organization we have described, from both the hindbrain and spinal cord, could represent an ancestral state, or it could represent a highly derived state that appeared at some point on the teleost lineage. The ability of the sensory neurons to exist between both the hindbrain and spinal cord organization suggests some degree of modularity, at least at larval stages. Prior comparative research across species has indicated a high degree of variability within sensory structures [126]. Regardless of its origins in evolutionary history, we propose that further work on the sensory innervation from the hindbrain FSNs could be used to interrogate the evolution of forelimb sensorimotor systems.

CHAPTER 3

THE PECTORAL FIN AS A SENSORY STRUCTURE: TERMINAL ANALYSIS ACROSS THE WHOLE FIN

3.1 Abstract

Limbs of animals perform a wide range of behaviors with sophisticated sensorimotor control. Sensation from the skin of the limb is an important component of sensory input, providing information on the external environment as well as on the limb itself. Here, I harnessed the genetic tools, small size, and optical clarity of larval zebrafish to examine the sensory terminals of the entire larval zebrafish pectoral fin. *Islet2B+* terminals appear all across the fin on both the medial and lateral surfaces of the fin. Initial examination of the whole population shows there are two terminal subtypes: simple free endings and varicosities. Examination of stochastically labeled *Tg[islet2b:Gal4]* transgenic fish injected with UAS:ptagRFP reveals that these terminal subtypes are found in single cells as well, indicating that terminals are intermingled on endings from just one cell. Analysis of the sensory terminals with respect to the functional subregions of the fin, the fin body and the fin membrane, reveals that the highest density of the sensory terminals are found on the skin of the fin body. In contrast, the highest densities of terminals from single cells were not found in specific locations on the fin. I used interterminal nearest neighbor distances to assess the degree of tiling between the population and the single cell sample. The interterminal distances between endings from a single cell were much larger than the interterminal distances calculated for the entire population indicating that neurons overlap significantly in their arborizations and possibly that the neurites of an individual cell self-avoid with a lower minimum terminal distances in the whole population. Finally, I characterize the terminal distributions around the blood vessel associated "joint" and the fin membrane margin, and I compare these distributions to an intermediate membrane midpoint as a control. There are significant biases towards the fin membrane in the population level analysis, despite there being no observable biases in distributions of terminals. This study characterizes terminal distributions across the entire fin surface,

and it provides a basis for future studies investigating sensorimotor integration.

3.2 Introduction

Sensory terminals embedded in the skin of animals are critical for sensory input that occurs on the skin. Work in a variety of animals has identified that the skin is densely packed with sensory terminals [123, 141, 25, 76, 80, 100, 56, 92, 11, 106, 21] reviewed in [62, 79, 103]. While I established the cell populations that innervate the pectoral fin (chapter 2), we do not yet have a full map of the sensory field of the fin itself. Here, I take a step toward building that sensory map by investigating terminal endings as the presumptive source of the major sensory input to afferents. I examined the distributions of terminal endings of both the fin sensory neurons (FSNs) identified in chapter 2 and the neurons from dorsal root ganglia (DRG neurons). Specifically, I interrogate how terminal afferent endings are distributed across the full population of sensory neurons innervating the fin.

The larval zebrafish is the ideal system within which to explore terminal distributions of a limb system. At mid to late larval stages, the pectoral fin is relatively large compared to the total axis length, but it has not yet developed into the complex structure of the adult zebrafish [39, 143]. The pectoral fins beat asynchronously during forward slow-swimming, and they are periodically active while the fish is stationary [142, 41]. During this time period, the fin is composed of two basic structures: the fin body (FB), composed of the endochondral disk surrounded by the adductor and abductor muscles, and the fin membrane (FM), composed of the actinotrichia and a thin membrane [143]. A blood vessel runs along the margin between these two regions. This simple organization is maintained throughout the late larval stages, with the transition to the adult fin morphology occurring much later, at roughly 23dpf [39].

As larval zebrafish actuate their fins, the fin bends at the position of the blood vessel [41, 40]. During fin abduction the FM folds in toward the body at the position of the blood vessel's distal margin, while in adduction the region remains straight and in line with the FB. Functionally, this "joint" is similar to the elbow join in tetrapods. In prior work (chapter 2), I examined sensory innervation with reference to significant regions of the fin related to this joint: the ventral FB,

ventral FM, dorsal FB, and dorsal FM. Surprisingly, I found that the branches of primary afferents were not organized with respect to this blood vessel location or the functional subregions of the fin. This result raised questions about how sensory terminals, the presumed site of sensation for the FSNs, are organized on the pectoral fin.

Here, I present a deep dive examination of the sensory terminals distributed across the skin of the pectoral fin. I took advantage of the larval zebrafish's small size and transgenic toolkit to examine terminals in the full fin-context. I sought to characterize the terminals over the full area of the pectoral fin surfaces and on both the medial and lateral sides of the fin. Using laser point scanning confocal microscopy, I acquired single micron optical sections across the entire pectoral fin. The single micron resolution allowed for clear differentiation between the medial and lateral surfaces of the fin at functionally interesting points. Finally, I utilize two different transgenic fish lines to sample both the entire sensory population in the fin and single cells with stochastic labeling.

Through these experiments, I sought to answer four specific questions to understand terminal ending distributions. First, how are sensory terminals distributed across the entire surface of the fin? Prior work investigating the distribution of serotonin positive cells on the caudal fins of zebrafish described a total of 10 putative sensory cells across the entire caudal fin [74]. This was a substantially lower number than would be reasonable given our results from chapter 2. Given the different developmental stages of the pectoral and caudal fins at 5dpf, I hypothesized there would be somewhere between 100 to 200 terminals on the pectoral fins. Next, I asked are terminals distributed at functionally important regions of the pectoral fin? I hypothesized that terminal distributions would be biased to the blood vessel separating the FM and the FB, based on the description of that region as the functional "joint." Furthermore, because the edges of the fin are highly flexible and positioned to optimally be involved in fluid mixing, I expected to find increased numbers of terminals around the very edge of the FM. Third, I ask about the distributions of terminals with respect to each other. Based on prior work in invertebrates and vertebrates (reviewed in [42, 162], I expected the spacing between terminals to be fairly uniform. Prior in-

vestigations of trigeminal sensory neurons in the head of larval zebrafish described avoidance between overlapping processes [128]. Based on this work, I expected that interterminal distances would be somewhat standardized, and furthermore that they would be consistent at the single cell level and the population level. Finally, I aggregate all these data and compare the sensory population with the single cell labeling. While this work primarily provides insight into the architecture of the sensory neuroanatomy of the pectoral fin, it also lays the groundwork for future functional investigations.

3.3 Materials and Methods

3.3.1 Fish

Animal use was approved by the University of Chicago's Institutional Animal Care and Use Committee. Adult zebrafish were maintained at 27°C on a 14/10 hour light/dark cycle in a custom fish facility. Fertilized eggs were held in 10% Hank's Solution in a 28.5°C incubator until 5dpf. At 5dpf, larval zebrafish were used for imaging studies and then euthanized in 0.02% 3-aminobenzoic acid ethyl ester (MS222, Sigma-Aldrich, St. Louis, MO, USA). To target sensory neurons, we used two transgenic lines that drive reporter expression in *islet2B*+ neurons [111, 102]. For initial studies examining the whole population, we used the *Tg[isl2b:GFP]*^{zc7} transgenic line (*Tg[islet2b:GFP]*) [111]. We subsequently used *Tg[islet2b:Gal4]*^{zc60} transgenic animals (gift from McLean Lab, Northwestern University, Evanston, IL, USA; [19]) to achieve sparse stochastic labeling [8, 90], enabling the reconstruction of individual neurons.

3.3.2 UAS construct injections

Embryos from *Tg[islet2b:Gal4]* transgenic fish were collected immediately following fertilization. These embryos were then transferred to an injection plate composed of a plastic dish with a microscopy slide taped to it. Using capillary action with a Kimwipe (Thermo Fisher Scientific, Waltham, MA, USA) on the opposite side, embryos were aligned against the slide. In this arrange-

ment, embryos at the one or two-cell stage were held stationary for DNA construct injections to generate stochastic labeling in the *Tg[islet2b:Gal4]* line with UAS:ptagRFP as described previously (gift from McLean Lab, Northwestern University, Evanston, IL, USA; [160, 90]). Following injections, embryos were transferred to fresh 10% Hanks and maintained at 28.5°C in a Fisher Scientific Low Temperature Incubator (Thermo Fisher Scientific, Waltham, MA, USA). After hatching at 3dpf, embryos were transferred to fresh Hanks and screened for single cell or sparse multicell labeling in the pectoral fin using a Leica MZFLIII dissecting scope (Leica Microsystems, Inc., Buffalo Grove, IL, USA) with a mercury lamp as the excitation source.

3.3.3 Imaging

Fish were transferred to a 24-well plate to track left or right pectoral fin innervation. At 5dpf, fish were anesthetized in 0.02% MS222 in Hanks, and mounted laterally in low-melt agarose as previously described [45]. In this study, we used a round 35mm dish with high precision No. 1.5 coverglass (MatTek Corporation, Ashland, MA, USA) for optimal signal. Embedded fish, with air from the swim bladder removed, were imaged on a Leica TCS SP8 II STED laser scanning confocal microscope (Leica Microsystems, Inc., Buffalo Grove, IL, USA) under Köhler illumination conditions. We used the White Light Laser set to 555nm as the excitation source, and the specimen was imaged through a 40x/1.30 NA oil immersion HC PlanApo objective. For RFP, the detector was a HyD tuned to 562nm to 700nm with gain set to 20 and gating turned on, and for visible light the detector was a PMT with gain set at 415. We used bidirectional scanning with phase adjusted at the beginning of each imaging session. Pinhole was set for 1 airy unit. For each fish, we imaged a 3x3 region with excitation gain turned on through a 150 to 250 micron z-stack for a total of nine stitched images of 1024x1024 pixels at 8-bit depth using LAS X software (Leica Microsystems, Inc., Buffalo Grove, IL, USA), stitched in the software with statistical blending between tiles, and saved as .lif files.

3.3.4 *Innervation reconstruction for single cells*

Whole z-stack tile scans were processed in Fiji [130, 131] using the Tubeness plugin [129] with a sigma value of 1. Output images were saved as 32-bit depth .tif files. We note that these files require substantial memory to open and work with. Post preprocessing for "tubes," we reconstructed the fin and axis innervation of 12 FSNs using the semi-automated Simple Neurite Tracer (SNT, version 3.1.3, [84]. SNT .traces files were exported as .swc files. These files were then read with the NeuoAnatomy Toolbox for Analysis of 3D Image Data (nat) package for R.

3.3.5 *Fin outlines*

To analyze the terminal distribution patterns within the fin, we digitized 18 points on the fins of brightfield images for each confocal z-stack. We then flattened these 18 points in order to examine the terminal distributions in 2D. We used the Bio-Formats importer [82] in Fiji [130, 131] to open the fluorescent and brightfield confocal z-stacks. We merged the two images together and used the multipoint function in Fiji to assign the 18 points in three-dimensional space: nine points on the outer edge of the FB as demarked by the blood vessel and nine points on the edge of the FM. Of each of these sets of nine points, two points were at the base, one on either side, one point was at the maximum distance from the base, and, on each side of that point, there were three points that roughly defined the shape of the fin.

3.3.6 *Fin terminal reconstructions and density mapping*

In SNT, we tagged the primary afferents of single cells to segregate them into medial surface innervation and lateral surface innervation. SNT .traces files for fin only reconstructions were loaded into FIJI for each fish. Reconstructions were exported as "tips" only to the ROI manager of FIJI. Once in the ROI manager, endpoints were measured for x and y position for both medial fin surface and lateral fin surface. For whole population sampling, terminals were marked through the 3D z-stack using the multi-point selection tool, then measured and z-stack location was dis-

carded. Individual terminals were separated out into medial and lateral fin surface positions by visual inspection of the brightfield and fluorescent image overlays. Two dimensional x and y data for each terminal point were mapped with the specific x and y dimensions of the fin for each individual fish using R. Densities were color coded with respect to the number of terminal points across the entire plot.

3.3.7 Nearest neighbor analysis of interterminal distance

The single cell terminals were assessed from the stochastic labeling in the *Tg[islet2b:Gal4]* transgenic fish, and the population terminals were assessed from the *Tg[islet2b:GFP]* transgenic fish. X and y coordinates for individual terminals were imported into R and tagged based on their fish ID number and their terminal "type." Each point was assigned the categorical value of "SC" for single cell or "pop" for population quantification. Using the Classes and Methods for Spatial Data (sp) and Interface to Geometry Engine Open Source (rgeos) packages in R, raw x and y coordinates were first transformed into spatial objects. I next assessed the minimum distance in microns between the second closest point to each starting terminal. The second point was assessed because the first closest point is the same terminal (i.e. closest terminal to the starting terminal is that terminal). Duplicate points were then removed. Minimum interterminal distances were analyzed between the single cell terminal samples and the population terminal samples, and they were compared using an ANOVA for both fin surfaces, the lateral fin surfaces, and the medial fin surfaces.

3.3.8 Fin margin, blood vessel margin, and intermediate midpoint analysis

I analyzed innervation of two hypothesized functional regions of the larval zebrafish pectoral fin: the fin margin on the fin membrane (FMM), the blood vessel margin (BVM), and an intermediate artificial boundary between the two, which we will term the membrane midpoint (MPM). Based on the hypotheses that the BVM and the FMM are functional subregions of the fin, the MPM should be a functionally insignificant intermediate between the two, therefore showing corre-

spondingly lower numbers of terminals. The FMM and BVM were assessed using the brightfield images from intact z-stacks in FIJI. Both margins were marked first with the multipoint function, and then they were traced with the freehand line tool. For terminal distribution analysis, terminals within 20 microns of the margins or the MPM were marked using the multipoint function. The FMM and BVM were traced from the proximal and ventral base of the fin. Once the FMM and BVM were traced, the MPM was marked using the multipoint function at an intermediate point midway between the FMM and the BVM on the fin membrane only. The MPM was traced all the way to the base of the fin for accurate length measurements, however terminals in this region were already assigned to either the FMM or BVM due to the fact that the fin membrane and blood vessel are within 20 microns of each other by the fin base. As result, there may be some under sampling of the MPM in the most proximal areas of the fin closer to the base of the fin, however these terminals are still captured by the FMM and BVM quantifications. The freehand line tool outlines were added to the ROI manager for accurate tracking of progress throughout the measurement process. Once all the terminals were marked, the freehand line tool was used to measure the lengths between the base of the fin and the first terminal. Then each subsequent terminal was measured based on its distance from the prior terminal. Then, using the overall length of the margin, each terminal was mapped according to the percentage of the length of the fin. The length of the fin begins at 0% at the proximal ventral fin base and continues around the outside of the respective margin, either FMM, BVM, or MPM, until it reaches 100% at the proximal most point on the dorsal edge of the fin base.

3.3.9 Figure preparation

I generated a duplicate set of microscopy images specifically for image preparation. Stitched, tiled z-stacks were projected along the z-axis, smoothed in Fiji, and flattened. I generated merged two channel images as well as z-depth color coded single channel images. When necessary, I cropped processed images for specific regions of interest. All graphs were generated in RStudio using ggplot2 [148]?. All figures were arranged in Adobe Illustrator (Adobe, San Jose, CA, USA).

3.4 Results

3.4.1 The islet2B neuron population has terminals all across the fin

I examined *Tg[islet2b:GFP]* to assess the sensory terminals across the entire fin. There are many terminals distributed across the skin from the surface of the FB to the FM. In both functional regions, there are two distinguishable terminal types: fine processes that end in simple free endings, and processes that terminate in enlarged varicosities. Along the FM, where the tissue is quite thin, the two types of terminals are clearly distinguishable in a single micron optical slice (Fig. 3.1 B). While two terminal subtypes were observed, distinct morphological differences between them could not be confirmed with the available methods. As a result, for the rest of the results we quantify both types of terminals together. Occasionally, at various points across the fin associated with both the FB and FM, a single process would exhibit two terminals in very close proximity to each other. This is discussed in more detail later.

Terminals in different regions appeared to exhibit different orientations with regards to their processes. Those towards the outer portion of the FM tended to be linear in organization, either appearing at the end of a single process or at the ends of two opposing branched processes (Fig. 3.1 grey outline marks the FMM, star corresponds with the enlarged portion from (A)). Overall, there are many terminals scattered across the FM. In contrast, terminals associated with the FB are rarely exhibited the linear organization of those on the FM. More often, terminals associated with the FB appeared to be on shorter branches off of longer processes. It was not possible to follow individual processes through this area due to substantial overlap of afferent branches among cells. Fluorescent terminals in single cell labeled samples showed the same terminal morphologies as whole cell population analysis, with varicosities on some endings and simple free nerve endings on others (Fig. 3.2). Because single cells were reconstructed, it is also possible to use the nat package in R to clearly visualize the entire reconstruction with labeled terminals (Fig. 3.2).

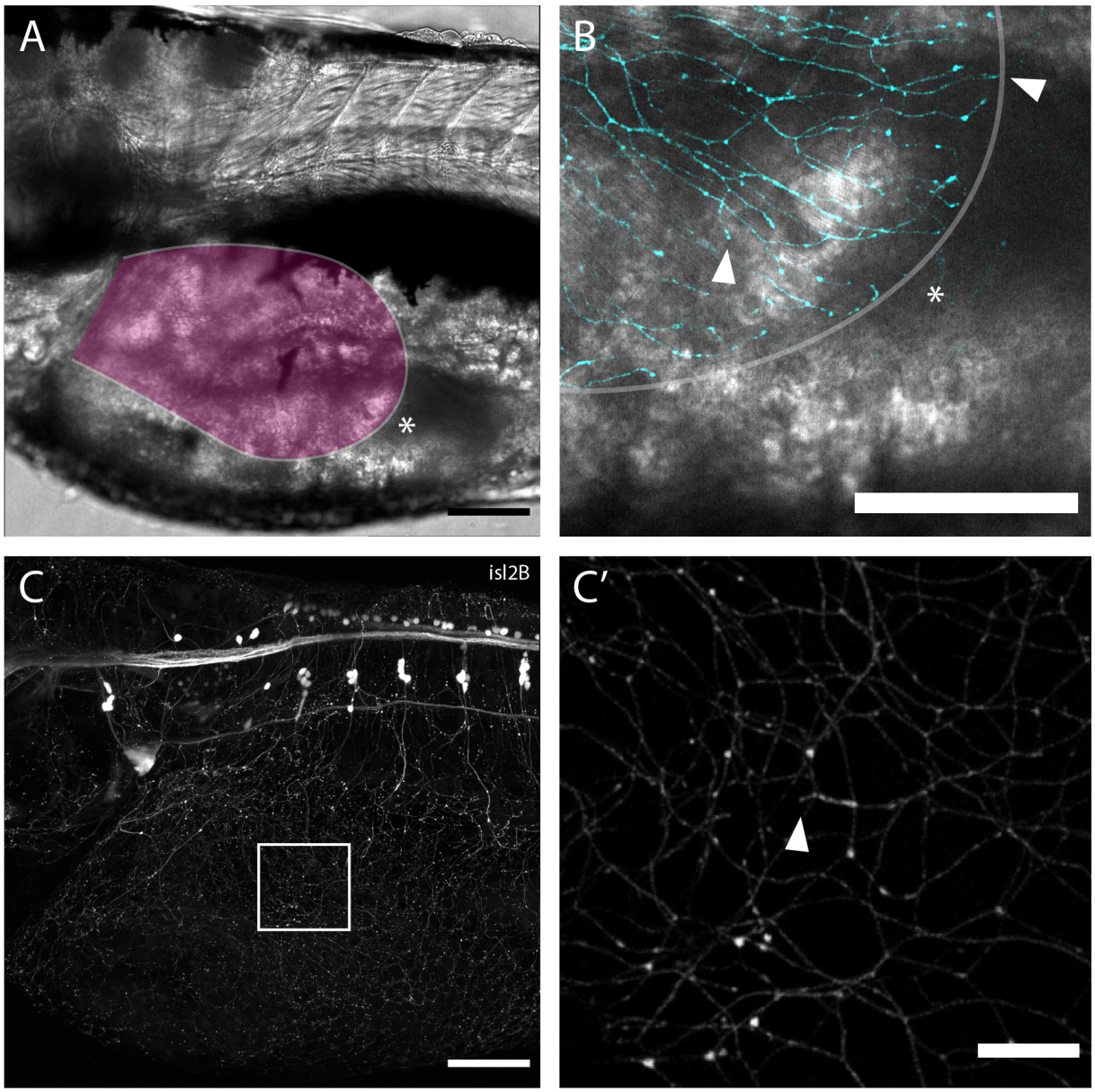

Figure 3.1: (A) Brightfield image of a 5dpf larval zebrafish with an overlay of the fin in pink, and a star highlighting an enlarged segment of the fin in B. (B) Magnified segment of the margin of the fin membrane, showing multiple terminals (some indicated with arrowheads), and the fin membrane margin is outlined in gray. (C) Fluorescent image of a lateral view of the fish in A, with a boxed region highlighting a portion of the fin magnified in C'. (C') A closer look at the terminal distributions associated with the fin body, which usually has terminals on short processes branched off of longer processes (arrowhead). Anterior is to the left, dorsal is up. Scale is 100μm in A and C, 50μm in B, and 20μ in C'.

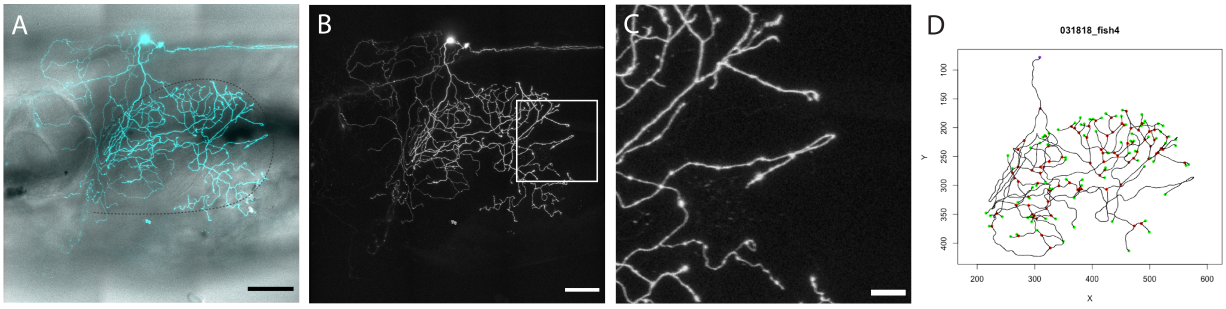

Figure 3.2: (A) Brightfield and fluorescent combined image showing a stochastically labeled neuron innervating the fin in a *Tg[islet2b:Gal4]* fish. Fin is bounded by a dotted line. (B) Brightfield image from A in isolation, in which the shape of the fin is visible by the cell innervation pattern alone. A box bounds the area enlarged in C. (C) Magnified image of the fin membrane from B highlights different terminal morphologies in the fin membrane. (D) A reconstructions from the nat package in R highlights terminals in green. Anterior is to the left, dorsal is up. Scale is 100μm in A, 75μm in B, and 20μm in C.

3.4.2 Whole population analysis reveals a small lateral to medial bias in terminal numbers

The surfaces of *Tg[islet2b:GFP]* fish pectoral fins have terminals distributed across the skin, and a majority of the terminals are concentrated on the FB (Fig. 3.3, n =3). I next investigated bias for the medial fin surface, as we observed when quantifying primary afferents in chapter 2. Both the lateral and the medial surfaces have distributions of terminals across the entire surface: on average, there are 642 ± 66 (mean $\pm$ SD) terminals on the entire fin (Fig. 3.3) (n = 3 fish). However, there are slightly lower densities of terminals on the medial fin surface compared to the lateral fin surface: there are an average of 283 ± 12 terminals on the medial surface of the fins compared to the 390 ± 51 terminals on the lateral surface (t-test, p = 0.022). On both medial and lateral surfaces, there is consistent distribution of terminals around the edges of the fin. To investigate the density of terminals, I generated heat maps showing the overlay of actual terminal locations with respect to fin points. The terminal densities of the whole population ranged from 0.010 to 0.012 terminals per μm^2 with a mean and standard deviation of 0.011 $\pm$ 0.0009 terminals per μm^2.

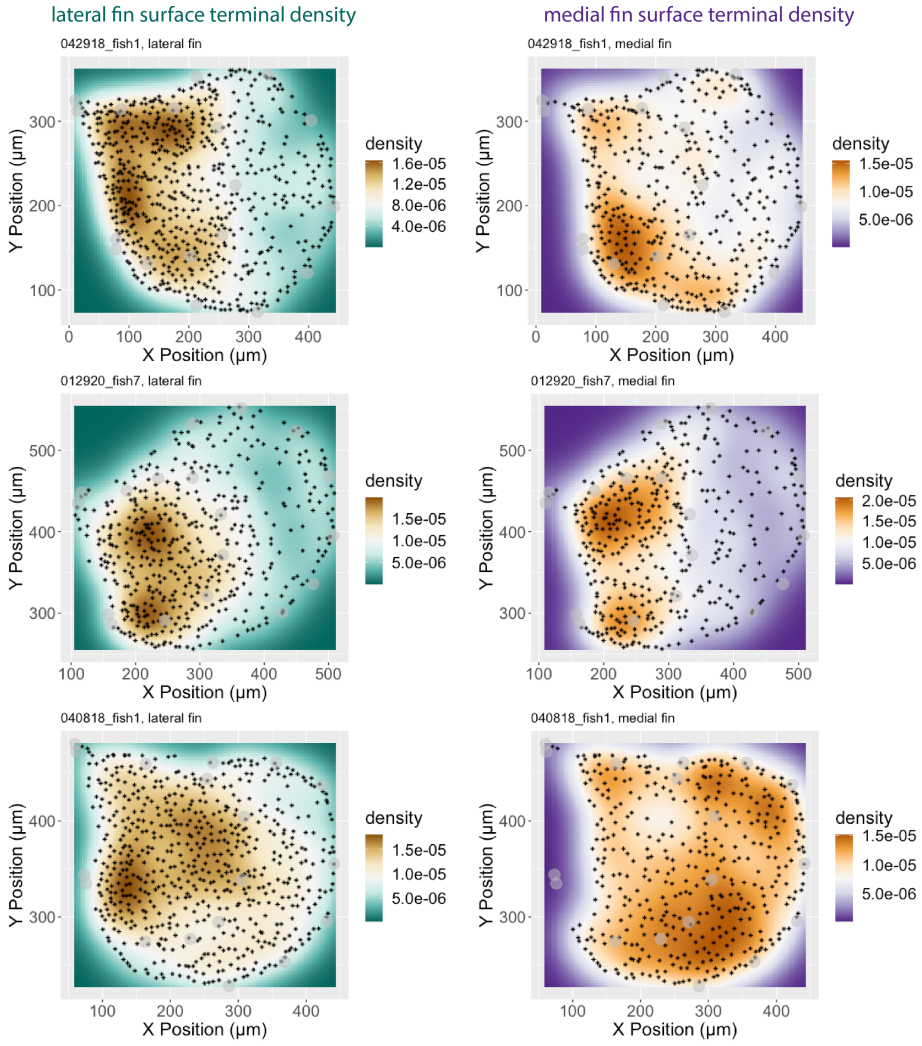

Figure 3.3: Terminals are scattered across the fin, and there are higher concentrations towards the proximal fin body, as bounded by the inner gray circles. The outer gray circles delineate the fin margin. Brown/orange distinguish higher terminal densities compared to green or purple regions. Left panel is the lateral fin surface, right panel is the medial fin surface.

3.4.3 *Single cell labeling shows that terminals from individual cells tend to be localized in the same regions of the fin*

For single cell labeling, the density maps were more varied. For best evaluation of terminal densities, I visualized density ranges specific for each fin. The distribution maps of terminals from single cells revealed that terminals tend to cluster together in the same region of the fin (Fig. 3.4) (n = 12). The density range for the *Tg[islet2b:Gal4]* was 0.00003 to 0.001 per μm^2. For the FM, individual neurons on the lateral fin surface had densities ranging from 0.00002 to 0.0006 terminals per micron. In contrast, the medial fin surface had densities ranging from 0.00007 to 0.0005 terminals per μm^2. For the FB, the lateral fin surface had terminal densities ranging from 0 to 0.0003 terminals per μm^2, and the medial fin surface had densities ranging from 0 to 0.0004 terminals per μm^2. For the most part, individual cells tended to have similar densities on the medial to lateral sides of the fin, although the density of the medial and lateral sides did not match up in three cases (Fig. 3.4). On average, the single cells label 30 ± 24.5 terminals (n = 12). For surface measurements on individual neurons there are insignificant differences with 14 ± 18 (mean $\pm$ SD) terminals on the lateral fin surface compared to an average of 18 ± 13 (mean $\pm$ SD) terminals on the medial fin surface (t-test, p = 0.296, n = 12).

3.4.4 *Interterminal distance shows that single cells tend to tile while the islet2B+ population does not*

The nearest neighbor interterminal distances of the single cell population terminals are significantly higher than the whole population interterminal distances (Pearson's Chi-squared, p < 0.001). This pattern holds true when examining the lateral fin surface (Pearson's Chi-squared, p = 0.001) and the medial fin surface (Pearson's Chi-squared, p = 0.003). The whole sensory neuron population has a nearest neighbor interterminal distance distribution ranging from a minimum of 0.311 to a maximum of 24.55 μm with a mean of 8.605 ± 3.271 μm and a median of 8.241 μm. In comparison, the single cell FSNs have a nearest neighbor interterminal distance distribution

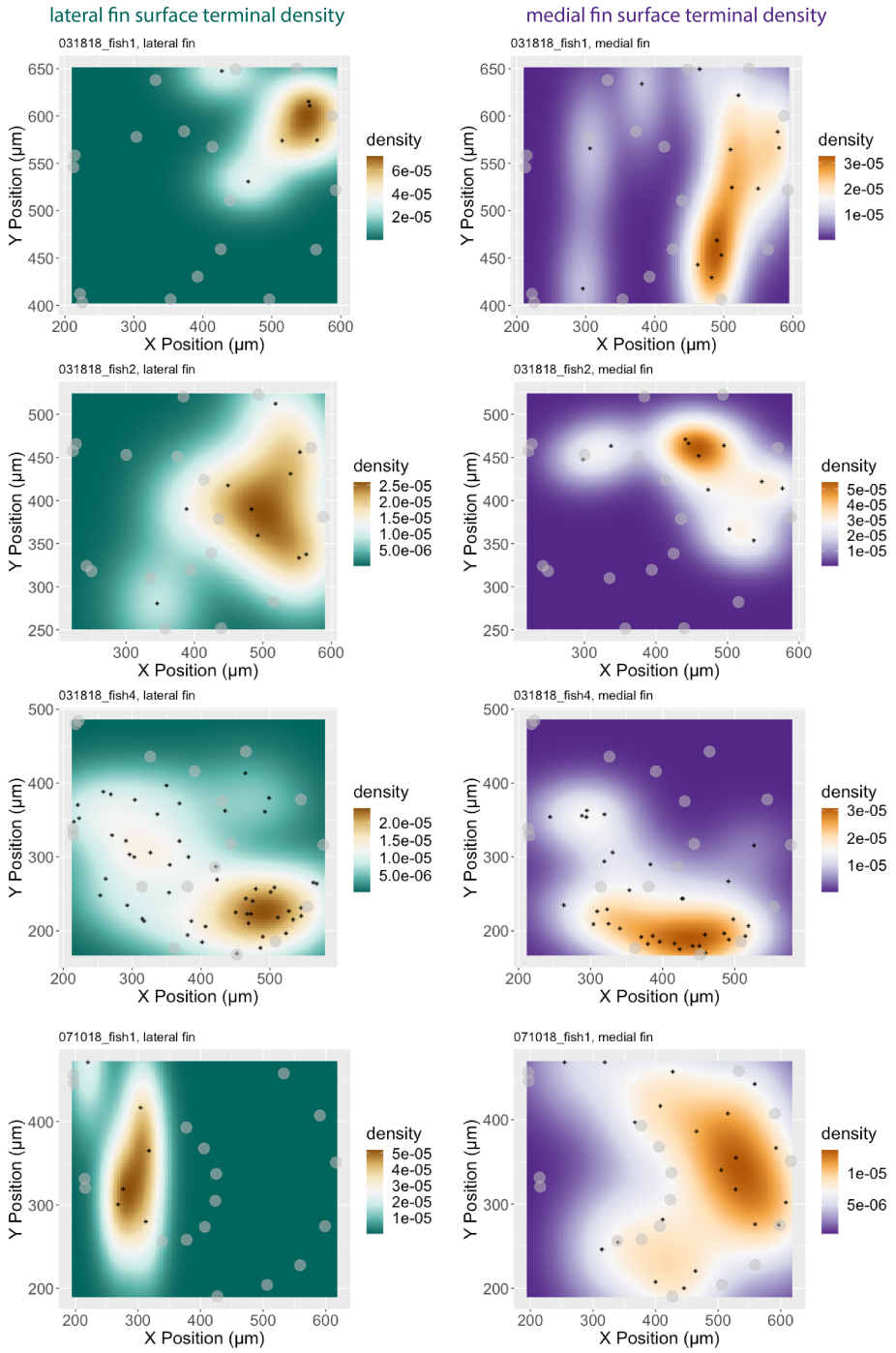

Figure 3.4: Single cell terminals tend to group together in different regions of the fin rather than spreading out across the entire fin. The outer gray circles delineate the fin margin. Brown/orange distinguish higher terminal densities compared to green or purple regions. Left panel is the lateral fin surface, right panel is the medial fin surface.

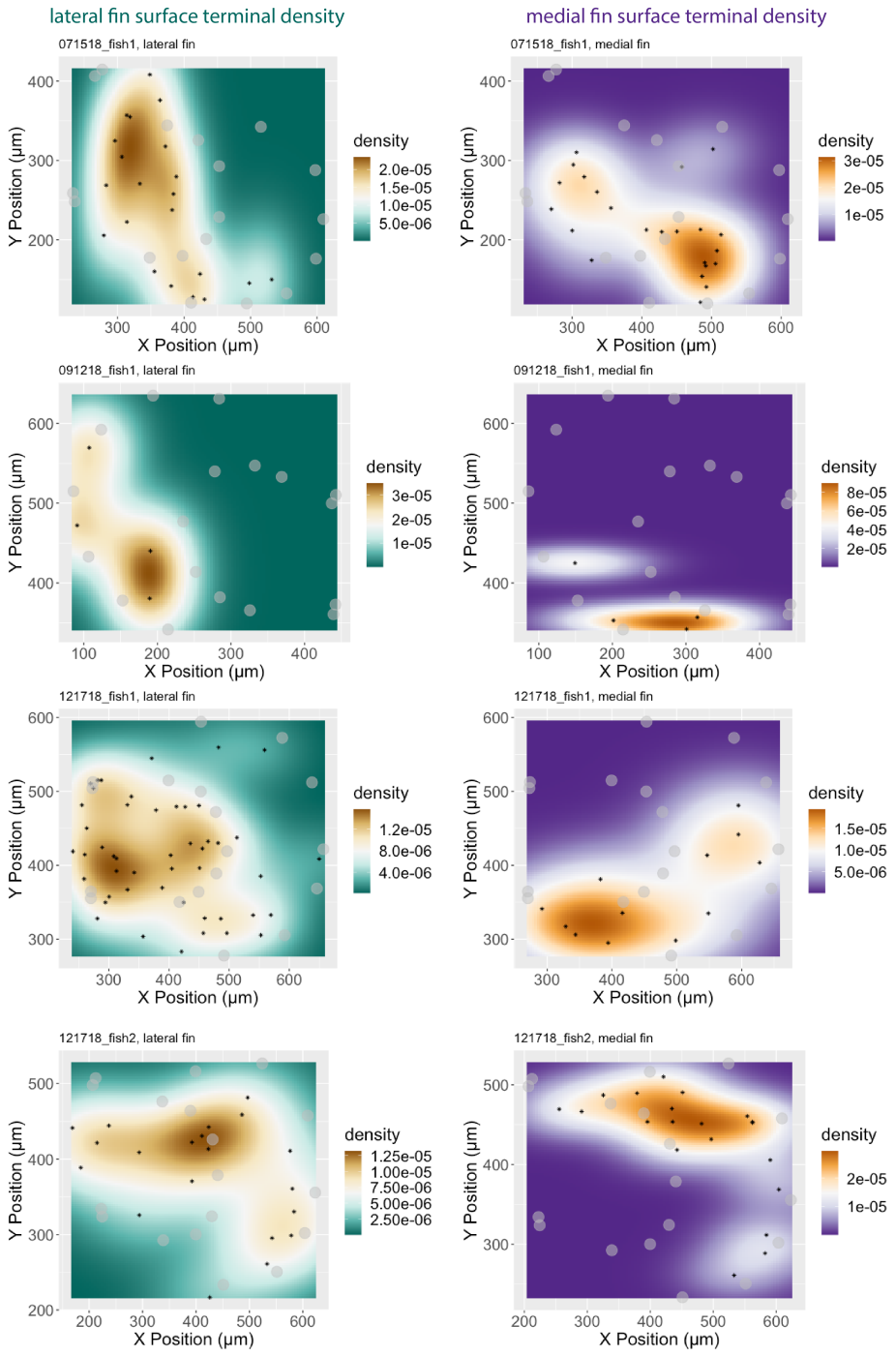

Figure 3.4, continued.

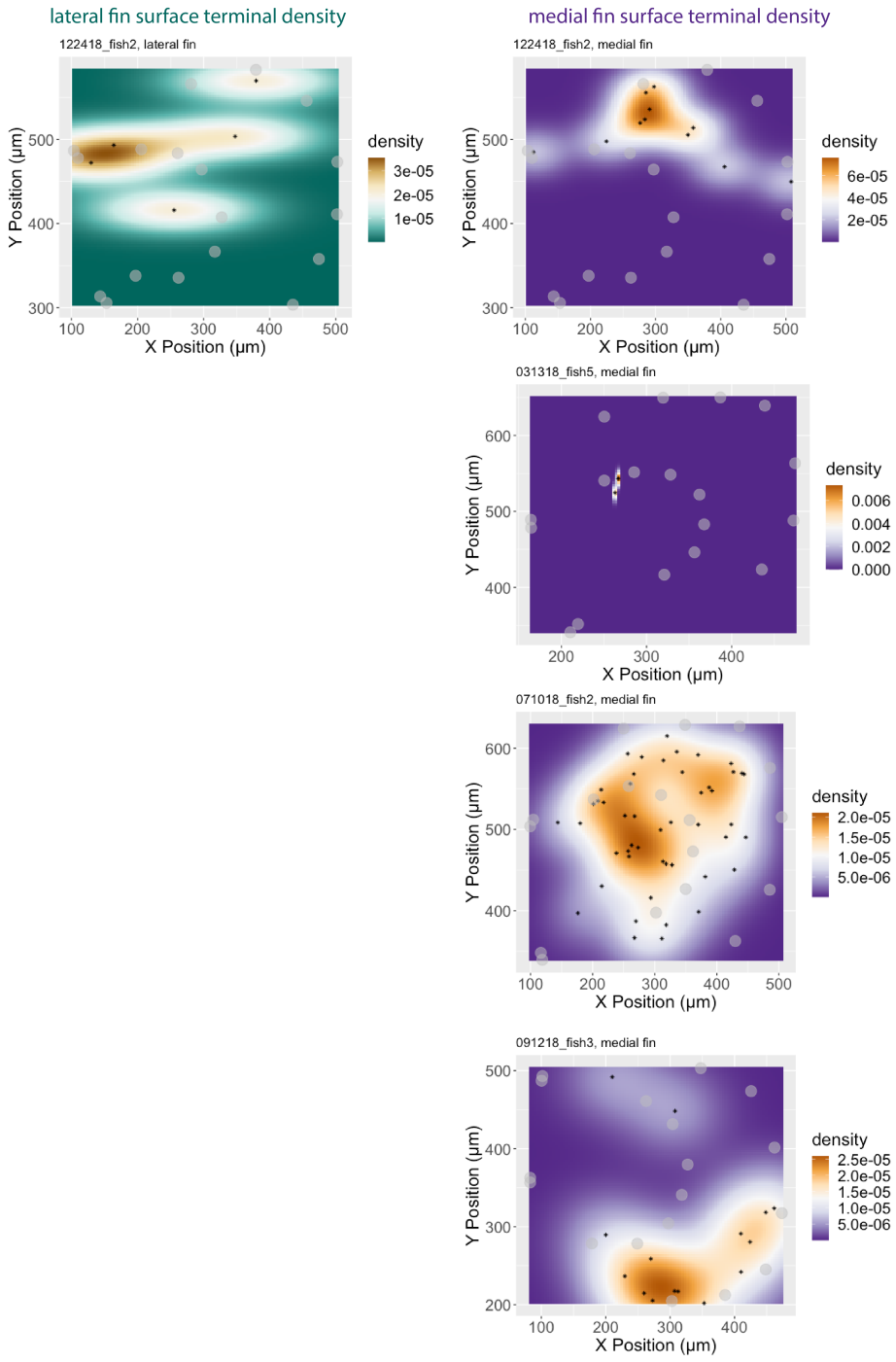

Figure 3.4, continued.

ranging from a minimum of 0.9386 to a maximum of 148.458 μm with a mean of 30.465 $\pm$23.411 μm and a median of 23.844 μm (Fig. 3.5). The whole population has a mean of 8.605 and a median of 8.241 μm. The single cells have a mean of 30.465 and a median of 23.844 μm. Taken together, these values suggest that a single neuron is sampling a large portion of the fin. Additionally, the much greater interterminal distance between the single cell endings and the population endings suggests that single neurons are tiling the fin and self-avoid to some degree, whereas the population does not.

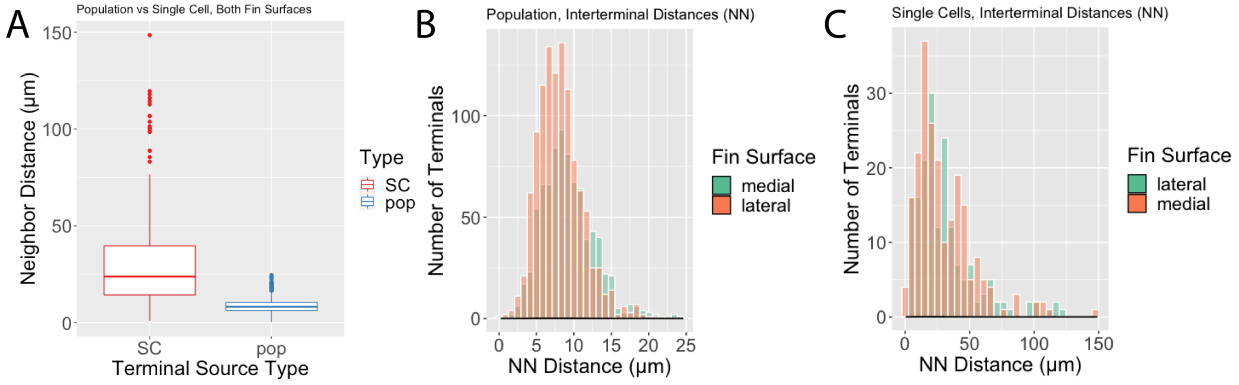

Figure 3.5: (A) Interterminal distances between nearest neighbors reveal the single cell (red, SC) terminals are significantly further from their nearest neighbors than the nearest neighbor terminals in the population (blue, pop). (B) Binned graph of the population interterminal distances show that most terminals are 5 to 10 μm away from each other. (C) Binned graph of the single cell interterminal distances show that most terminals are 10 to 30 μm away from each other. These patterns are consistent across the medial (green) and lateral (orange) fin surfaces for both groups.

3.4.5 Terminals are evenly distributed around two functionally significant margins, but they differ in densities

Distributions around the FMM are fairly comparable in *Tg[islet2b:GFP]* fish (min: 1%, Q1: 31%, median: 57%, mean: 55%, Q3: 81%, max: 99%) (Fig. 3.6) and in single cells of *Tg[islet2b:Gal4]* fish (min: 0%, Q1: 39%, median: 64%, mean: 57%, Q3: 78%, max: 99%) (Fig. 3.6). This corresponds to the proximal dorsal portion of the FM. The BVM also has an even distribution in the whole population with a flat distribution curve (min: 1%, Q1: 30%, median: 49%, mean: 49%, Q3: 70%, max: 98%) (Fig. 3.7), but the distribution of terminals around the BVM is slightly biased in the

single cell sample (min: 2%, Q1: 24%, median: 46%, mean: 49%, Q3: 71%, max: 98%) (Fig. 3.7). For the intermediate MPM, I analyzed the middle portion of the membrane to establish terminal distributions across a line that was not on a functionally significant boundary. The distributions in the whole cell population had a midpoint peak (min: 25%, Q1: 41%, median: 56%, mean: 55%, Q3: 68%, max: 91%) (Fig. 3.8), and the single cell labeling had a similar, albeit more exaggerated peak (min: 26%, Q1: 38%, median: 52%, mean: 52%, Q3: 63%, max: 87%) (Fig. 3.8). Distribution patterns for the BVM and MPM were consistent across medial and lateral fin surfaces. I found no key differences between the distributions of terminals for either FMM or BVM and the control MPM. This raised the question about terminal densities around these margins.

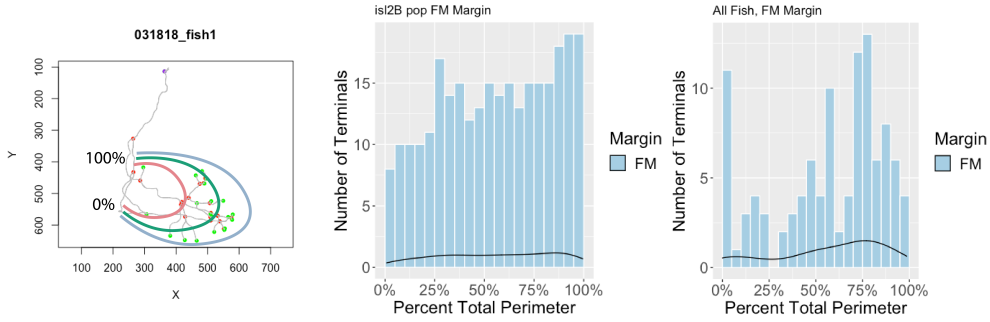

Figure 3.6: A reconstruction from the nat package in R highlights terminals in green, and overlays signify the fin membrane (blue), blood vessel (red), and midpoint membrane (green). Middle panel shows the distribution of terminals around the fin membrane of the population of all *islet2B+* terminals. Right panel shows the distribution of terminals around the fin membrane of stochastically labeled cells.

The *Tg[islet2b:GFP]* fish have terminal densities that are biased to the FMM with 0.093 terminals per micron. In comparison, the BVM only has a density of 0.008 terminals per μm, and the control MPM has a density of 0.016 terminals per μm (n =3). The densities at the FMM and the MPM were not significantly different (p = 0.305, n = 3), however, the densities of terminals at the BVM was significantly lower than the MPM (p = 0.0007, n = 3). This effect was maintained when examining the medial fin surface and the lateral fin surface in isolation (p = 0.002 for medial, p = 0.0003 for lateral, n = 3). Interestingly, the density trends around the FMM, BVM, and MPM were not maintained in the single cell samples of the *Tg[islet2b:Gal4]* fish. For the FMM, the terminal density was 0.009 terminals per μm (n =12). The BVM and MPM densities were 0.010 and 0.007

terminals per μm, respectively (n =12). These values were not significantly from each other (p = 0.207 for FMM and MPM, p = 0.127 for BVM and MPM). These results suggest that, in the population, the terminals are biased towards the fin membrane, especially towards the FMM. This trend is reflected by the much lower densities around the BVM as well. The fact that the single cell labeling doesn't show the same biases suggests that the terminals of single cells are not biased toward functional regions.

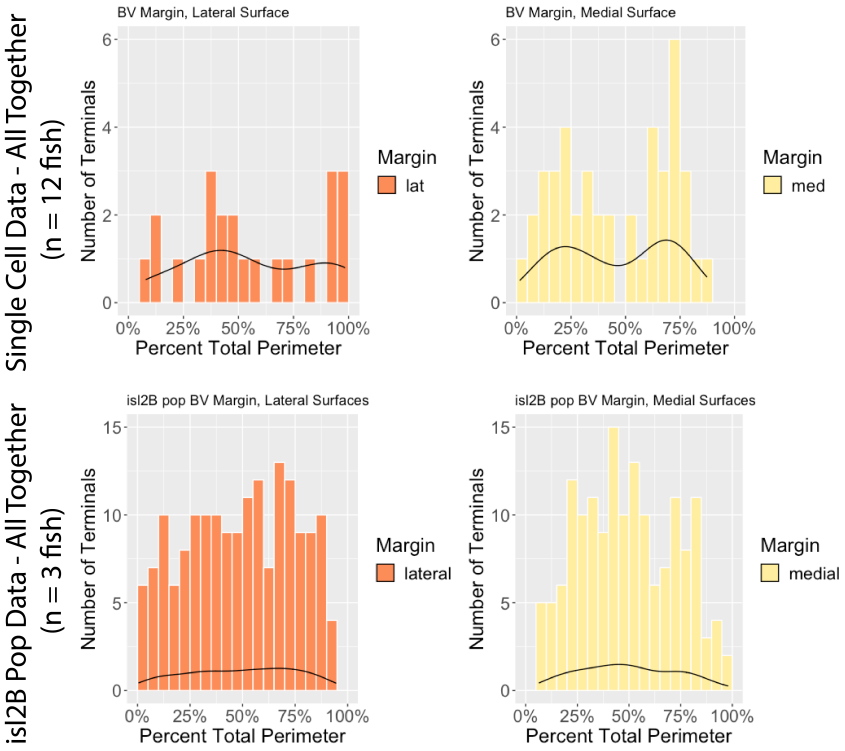

Figure 3.7: Left panel shows the distribution of terminals around the lateral surface associated with the blood vessel of the single cell sample (top panel) and the whole population (bottom panel). Right panel plots the distribution of terminals around the medial surface.

3.5 Discussion

In this chapter, I analyzed the terminal distributions in the 5dpf larval zebrafish pectoral fin. My prior work examining single cell labeling in stochastically labeled *Tg[islet2b:Gal4]* transgenic fish revealed extensive innervation of the pectoral fin by single cells, but that research left questions about the organization of sensory endings from the entire population. Owing to the substantial

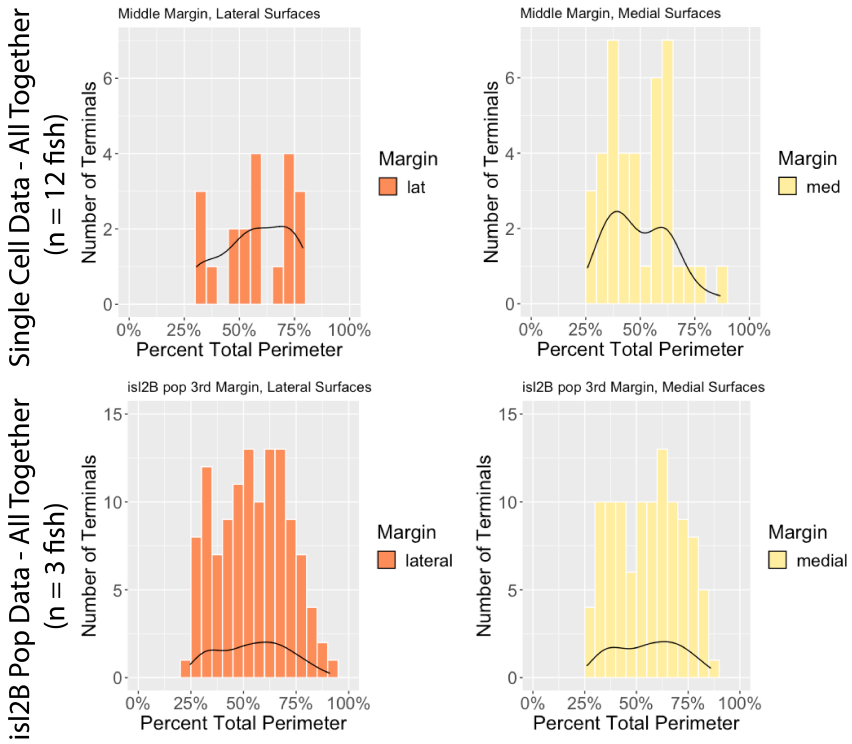

Figure 3.8: Left panel shows the distribution of terminals around the lateral surface associated with the membrane midpoint of the single cell sample (top panel) and the whole population (bottom panel). Right panel plots the distribution of terminals around the medial surface.

overlap in processes, it was not possible to use the *Tg[islet2b:GFP]* to analyze the entire pectoral fin as a sensory structure. As an alternative to examining primary afferents, here I have examined terminals in the pectoral fin as an approach to explore the sensory structure of a whole limb. I demonstrate that the pectoral fin is covered by sensory terminals on both the medial and lateral surfaces. These terminals are closely associated with each other across the entire *islet2B+* population, and they have a slightly sparser distribution within single cells. This sparseness in the single cells suggests some degree of tiling at the level of individual neurons. Additionally, I found that sensory terminals are not biased in their distributions around the two functional fin margins examined. These results provide better context for the hindbrain (HB) and Rohon-Beard (RB) fin sensory neurons (FSNs) identified in chapter 2. Physiological studies may provide further insights into the exact sensory function of the fin at this stage.

3.5.1 *Two different terminal morphologies on the fin suggest possible functional subtypes*

I observed two different subtypes of endings on the cutaneous sensory neurons in the fin while examining the entire population in the *Tg[islet2b:GFP]* fish. Often, sensory subtypes in the skin can be distinguished by their terminal anatomy (reviewed in [121]). Based on this, I investigated the terminals in stochastically labeled single neurons using the *Tg[islet2b:Gal4]* transgenic line. Surprisingly, we found that single cells have intermixed terminals of both morphologies. While it is possible that these observed morphological differences are due to neuroanatomical differences that result in higher aggregations of fluorescent protein at the site of the observed varicosities, I propose a different explanation.

An alternative hypothesis is that these neurons are multimodal: chemosensory, nociceptive, or mechanosensory. In a variety of invertebrate and vertebrate systems, single sensory neurons have been shown to be functionally responsive to multiple sensory stimuli [49, 133, 154, 66]. In some cases, taste bud chemoreceptors are also responsive to thermal stimuli [154]. In invertebrates, specialized sensors detect both innocuous mechanosensory input as well as harmful thermal stimuli [107]. Furthermore, prior work in adult fish has shown that the skin is covered in taste buds [46, 70]. Multimodal primary sensors have not yet been identified in fish fins; however, the larval zebrafish system holds promise as an *in vivo* system to explore how neuroanatomy may shed light on a potentially multimodal group of cells.

3.5.2 *High numbers of terminals suggest extensive DRG neuron innervation at 5dpf*

Based on prior neuroanatomical work investigating the innervation of FSNs into the pectoral fin, it is possible to estimate a rough number of DRG neurons innervating the fins. In chapter 2, we identified that there are between six and eight RB FSNs and two to seven HB FSNs that could be innervating the fin in any one fish. If we assume the maximum number of FSNs are present

and innervating the fin, there are 15 FSNs innervating the fin in one animal. Those cells have an average of 38 terminals on each single cell, for a total of 570 terminals across FSNs. Given that the *islet2B+* population has an average of 677, there are about 107 terminals that are unaccounted for by the FSN population. This gap between the single cell labeling and the population labeling could be filled by DRG neurons, and this difference suggests that DRG neurons are contributing to the fin sensory population together with FSNs.

Observations regarding the terminals revealed a surprisingly high number of terminals at the population level. In particular, we note a higher number of terminals on the lateral surface of the fin compared to the medial surface of the fin. This is in contrast to the single cell labeling, which reveals the opposite ratio. Notably, the single cell labeling fails to label DRG neurons. This suggests that the increase in the number of terminals on the lateral side could be due to higher DRG neuron innervation. Exploring this suggestion will require reliable labeling of single DRG neuron neurons, something we have not been able to accomplish with the *Tg[islet2b:Gal4]* transgenic line.

3.5.3 Preliminary exploration of tiling in a fish limb

Prior work has identified that neurons of the same subclass tend to self-avoid and "tile" in the skin of invertebrates and vertebrates [76] reviewed in [42, 21]. Low-threshold mechanoreceptors in mammalian skin show little to no overlap within subclasses, however a small area of the skin will be innervated by multiple individual neurons from different subtypes [76]. In my examination of the whole population of sensory neurons in the *Tg[islet2b:GFP]* and the single cells in *Tg[islet2b:Gal4]* fish, I find that there are substantially lower interterminal distances between terminals in the population compared to the single cell labeling. This result suggests that there is some degree of self-avoidance in single neurons. Prior work in zebrafish has indicated tiling between RBs and trigeminal neurons in the head [128], however my work in chapter 2 suggests intermingling between HB FSNs and RB FSNs. Future work will need to identify whether or not tiling is a result of distinct genetic or functional subclasses of sensory neurons.

Ultimately, this research into terminals lays exciting groundwork to further explore FSNs. Further investigation of the two different terminal morphologies could lend insights into their ultrastructure and function. Verifying that there are true subtypes of terminals would require electron microscopy. This level of examination would establish structural differences at the endings of the processes. As mentioned previously, electrophysiological and behavioral studies in the Hale Lab exploring the potential mechanosensitivity in the larval zebrafish pectoral fins were unsuccessful. Larval fish pectoral fins do not exhibit a clear response to touch either in fictive preps or free swimming behavioral tests. These observations, however, do not rule out alternative mechanosensory functions such as sensitivity to stretch or fluid flow on the fin membrane. Following confirmation of the terminal structure, next steps could include functional explorations at both the single cell and population level.

CHAPTER 4

DISCUSSION

In this thesis, I sought to explore the pectoral fin as a sensory structure and to establish the neuroanatomy of its associated sensory neurons. The major findings of chapter 2 revealed that, like the fin motor population [86], the sensory neurons originate in both the hindbrain and the spinal cord. This organization is a stark contrast to the mammalian vertebrate body plan, which has forelimb sensors originating solely from post cranial peripheral ganglia [139]. I also found that FSNs innervate both the pectoral fin and the axis in the immediate area around the fin, and they do so without somatotopic organization. This unusually broad spatial distribution suggests that FSNs are not only sensing input to the fin. The entire group of FSNs forms two clusters based on morphological parameters, which provides evidence for neuronal subtypes across the HB and RB FSNs as a population. In chapter 3, I investigated the terminal distributions across the entire pectoral fin. Population level analysis revealed that the pectoral fin is covered with densely grouped terminals. Comparison of single cell interterminal distances to population level interterminal distances suggests some tiling and self-avoidance within a single cell. Distributions around two functional margins, the FMM and the BVM, were not different from distributions around a control midpoint. This result further supports a lack of functional organization as identified in chapter 2. Taken together, all these results suggest that FSNs are not mechanosensors for specific regions of the fin. Furthermore, this work raises interesting ideas for future experiments, which I will elaborate on more below.

4.1 The pectoral fin as a sensory structure

Prior work in fish has explored the pectoral fin as a sensory structure in adult fishes. Hardy et al. identified mechanosensory responses in the fins of adult *Pimedlodus pictus*, a benthic species of catfish living close to the substrate in murky water [47]. Interestingly, this study revealed that sensory innervation in the fin was associated with putative mechanosensors in the membrane

between the fin rays [47]. Studies in a variety of fish species have identified that different environmental demands create different sensory organizations in fins [31, 135, 96, 4, 78]. This is true in both benthic species and pelagic species swimming in open water [151, 3]. Sensory feedback from paired appendages clearly plays a more significant role in adult fishes than previously thought; however exploration of the integration into spinal circuitry is not tractable in adult fish.

The larval zebrafish system presents the ideal platform with which to explore sensory neuroanatomy and broader circuit integration. Here, I conducted an exploration of the primary afferents in the pectoral fin as well as their sensory terminals. Based on my results, we have been able to establish that the entire pectoral fin is densely innervated by single cells that together form a population covering both the medial and lateral surfaces. Future work can also elaborate on the functional integration of FSNs into fin circuitry. Studies of axial RBs have identified their secondary targets as pre-motor interneurons [22, 57, 145, 71, 83], but the far anterior location of the HB FSNs could mean they have different synaptic partners. As described previously, the pectoral fin motor pool is also a mixed population that spans the posterior hindbrain and the anterior spinal cord [87], and this motor pool seems like a logical starting point for either calcium imaging or optogenetic manipulations. There is also some possibility for circuit overlap with axial-only RBs and those that are FSNs, however it seems unlikely that the hindbrain FSNs are innervating local spinal circuits. Instead, perhaps the FSNs in the HB are targeting the local rhythmic circuits in the hindbrain [14, 87]. Given the involvement of the fin in fluid mixing [40], this seems like a plausible direction for future functional exploration.

4.2 Changing demands through ontogeny could be reflected in changes in sensory structures

The functional constraints on the adult and larval pectoral fins raises interesting questions about sensation in these different life stages. In my thesis work, I clarify the population of neurons providing dense innervation of the fin prior to the development of fin rays [39]. Much of the

prior work in fish fin sensation has been conducted in adults, however work in the Hale Lab has never conclusively identified mechanosensory responses in pectoral fins of larval zebrafish either through behavioral or functional studies. At the larval stages, zebrafish experience different functional constraints. Notably, they require cutaneous respiration rather than gill-based respiration (reviewed in [44]). Prior functional studies in a variety of larval species have identified increased pectoral fin beats and/or increased swimming bouts in hypoxic environments [59, 60, 41]. These behaviors are the aquatic vertebrate equivalent of lengthened breathing cycles in the presence of high CO_2 environments in birds [23]. Relating behavioral results in zebrafish to pectoral fins and FSNs will require both immunofluorescent experiments and functional interrogation at the cellular level.

There is plentiful evidence for oxygen sensing cells in a variety of fish species. Both amphibious and air-breathing fish species have specialized neuroepithelial cells (NECs) on their gills and skin [157, 119, 156]. These NECs are serotonin positive, and a similar type of cells has been found on zebrafish before the development of gills [65]. By adulthood, zebrafish have putative oxygen sensors all across their gills [158, 112, 26, 63]. Given the role of pectoral fins in circulating oxygenated water around the skin for cutaneous respiration, it would make sense that there may be oxygen sensitive sensors on the fin. Future studies could examine markers associated with oxygen sensing cells, and functional studies could target the FSN population for calcium imaging experiments exploring responses to hypoxic environments.

We can draw additional comparisons between larval zebrafish and soft-bodied insect larvae. Like fish, insects undergo a metamorphosis between the larval stages and the adult stages. Interestingly, larval insects exhibit different primary afferent structures as well as function [140]. There is evidence that sensory neurons, specifically mechanosensors, may actually play a direct role in metamorphosis [101, 137]. Zebrafish also undergo substantial anatomical changes between larval and adult stages [143, 39, 108]. Prior work has revealed that the cell death of RBs is decoupled from the development of DRG neurons [149], and we observed DRG neurons innervating the fin during the examination of *Tg[islet2b:GFP]*. Understanding the timing of FSN transition

throughout ontogeny is feasible with genetic manipulations and observational studies, however exploring their involvement in metamorphosis would require more directed manipulations.

Unraveling the sensory modality for these FSNs will necessitate functional studies to examine responses in different conditions. This is especially relevant if these cells are multimodal. Prior work has begun to explore the role of pectoral fins in fluid mixing [41], and these studies could be incorporated into physiological studies. Due to the nature of the extensive axial innervation, I do not think electrophysiological studies will be possible in the FSN population. Instead, I propose that calcium imaging studies could be fruitful for exploring sensory responses. These experiments could utilize newer genetically encoded calcium indicators with heightened sensitivities and/or faster kinetics to image the responses of these cells in oxygen deprivation experiments. Nociceptive responses can also be explored with mustard oil or pharmacological applications. Conclusive chemosensitive or nociceptive responses would allow for more in depth exploration of the lack of response to mechanosensory stimuli as well.

4.3 Future work will need to explore DRG neuron innervation

Finally, while we have not been able to gain the necessary single cell resolution to fully explore this result, we have identified that DRG neurons are innervating the surface of the fin at 5dpf. Prior work in adult sea robins has characterized a derived organization of the DRG neurons fused with the dorsal horn of the spinal cord [31, 32]. This organization is in contrast to all other studied vertebrates where the DRG neurons are a separate cluster of neurons completely distinct from the spinal cord. In the sea robin, the "accessory lobes" are associated with specialized free fin rays [31, 32]. This represents a certain modularity of peripheral sensory neurons and how they integrate with the spinal cord. Once the DRG neuron innervation of the larval zebrafish pectoral fins are characterized, this model system could be used for evolutionary developmental biology studies. Specifically, the pectoral fins would be an ideal system in which to explore the modularity of this sensory system.

More broadly, a fuller picture of the sensory innervation of the pectoral fin will be useful

for regeneration studies. Zebrafish are a popular model organism for this work because they are capable of regenerating their pectoral fins, and studies have shown that peripheral nerve innervation is critical for adequate regeneration of paired limbs [136]. More recent work has found that zebrafish lose their ability to regenerate their pectoral fins through ontogeny [155]. Exploration of the relationship between pectoral fin sensory innervation and these regenerative processes could shed light on future clinical directions for a variety of pathologies or even integration of sensory feedback into prosthetics [132].

REFERENCES

[1] V. E. Abraira, E. D. Kuehn, A. M. Chirila, M. W. Springel, A. A. Toliver, A. L. Zimmerman, L. L. Orefice, K. A. Boyle, L. Bai, B. J. Song, K. A. Bashista, T. G. O'Neill, J. Zhuo, C. Tsan, J. Hoynoski, M. Rutlin, L. Kus, V. Niederkofler, M. Watanabe, S. M. Dymecki, S. B. Nelson, N. Heintz, D. I. Hughes, and D. D. Ginty. The Cellular and Synaptic Architecture of the Mechanosensory Dorsal Horn. *Cell*, 168(1-2):295–310, Jan 2017.

[2] B. R. Aiello, A. M. Olsen, C. E. Mathis, M. W. Westneat, and M. E. Hale. Pectoral fin kinematics and motor patterns are shaped by fin ray mechanosensation during steady swimming in Scarus quoyi. *J. Exp. Biol.*, 223(Pt 2), 01 2020.

[3] B. R. Aiello, T. A. Stewart, and M. E. Hale. Mechanosensation in an adipose fin. *Proc. Biol. Sci.*, 283(1826):20152794, Mar 2016.

[4] B. R. Aiello, M. W. Westneat, and M. E. Hale. Mechanosensation is evolutionarily tuned to locomotor mechanics. *Proc. Natl. Acad. Sci. U.S.A.*, 114(17):4459–4464, Apr 2017.

[5] A. A. Akerberg, S. Stewart, and K. Stankunas. Spatial and temporal control of transgene expression in zebrafish. *PLoS ONE*, 9(3):e92217, 2014.

[6] R. G. Almeida and D. A. Lyons. Intersectional Gene Expression in Zebrafish Using the Split KalTA4 System. *Zebrafish*, 12(6):377–386, Dec 2015.

[7] M. An, R. Luo, and P. D. Henion. Differentiation and maturation of zebrafish dorsal root and sympathetic ganglion neurons. *J. Comp. Neurol.*, 446(3):267–275, May 2002.

[8] K. Asakawa, M. L. Suster, K. Mizusawa, S. Nagayoshi, T. Kotani, A. Urasaki, Y. Kishimoto, M. Hibi, and K. Kawakami. Genetic dissection of neural circuits by Tol2 transposon-mediated Gal4 gene and enhancer trapping in zebrafish. *Proc. Natl. Acad. Sci. U.S.A.*, 105(4):1255–1260, Jan 2008.

[9] G. A. Ascoli, D. E. Donohue, and M. Halavi. NeuroMorpho.Org: a central resource for neuronal morphologies. *J. Neurosci.*, 27(35):9247–9251, Aug 2007.

[10] E. Azim, J. Jiang, B. Alstermark, and T. M. Jessell. Skilled reaching relies on a V2a propriospinal internal copy circuit. *Nature*, 508(7496):357–363, Apr 2014.

[11] L. Bai, B. P. Lehnert, J. Liu, N. L. Neubarth, T. L. Dickendesher, P. H. Nwe, C. Cassidy, C. J. Woodbury, and D. D. Ginty. Genetic Identification of an Expansive Mechanoreceptor Sensitive to Skin Stroking. *Cell*, 163(7):1783–1795, Dec 2015.

[12] J. E. Bardach and J. Case. Sensory capabilities of the modified fins of squirrel hake (Urophycis chuss) and searobins (Prionotus carolinus and P. evolans). *Copeia*, 2:194–206, Jun 1965.

[13] A. H. Bass and B. P. Chagnaud. Shared developmental and evolutionary origins for neural basis of vocal-acoustic and pectoral-gestural signaling. *Proc. Natl. Acad. Sci. U.S.A.*, 109 Suppl 1:10677–10684, Jun 2012.

[14] A. H. Bass, E. H. Gilland, and R. Baker. Evolutionary origins for social vocalization in a vertebrate hindbrain-spinal compartment. *Science*, 321(5887):417–421, Jul 2008.

[15] J. Beard. On the early development of Lepidosteus osseu. *Proc. Roy. Soc.*, 46:108–118, 1889.

[16] J. Beard. The transient ganglion cells and their nerves in Raja batis. *Anat. Anz.*, 7:191–206, 1892.

[17] J. Beard. The history of a transient nervous apparatus in certain Ichthyopsida. An account of the development and degeneration of ganglion-cells and nerve fibres. *Zool. JahrbÃijchÃl'r Abt. Morphol.*, 1896.

[18] S. Bello-Rojas, A. E. Istrate, S. Kishore, and D. L. McLean. Central and peripheral innervation patterns of defined axial motor units in larval zebrafish. *J. Comp. Neurol.*, 527(15):2557–2572, 10 2019.

[19] N. Ben Fredj, S. Hammond, H. Otsuna, C. B. Chien, J. Burrone, and M. P. Meyer. Synaptic activity and activity-dependent competition regulates axon arbor maturation, growth arrest, and territory in the retinotectal projection. *J. Neurosci.*, 30(32):10939–10951, Aug 2010.

[20] R. R. Bernhardt, A. B. Chitnis, L. Lindamer, and J. Y. Kuwada. Identification of spinal neurons in the embryonic and larval zebrafish. *J. Comp. Neurol.*, 302(3):603–616, Dec 1990.

[21] S. E. Blackshaw. Morphology and distribution of touch cell terminals in the skin of the leech. *J. Physiol. (Lond.)*, 320:219–228, Nov 1981.

[22] U. L. Bőhm, A. Prendergast, L. Djenoune, S. Nunes Figueiredo, J. Gomez, C. Stokes, S. Kaiser, M. Suster, K. Kawakami, M. Charpentier, J. P. Concordet, J. P. Rio, F. Del Bene, and C. Wyart. CSF-contacting neurons regulate locomotion by relaying mechanical stimuli to spinal circuits. *Nat Commun*, 7:10866, Mar 2016.

[23] P. Bouverot. Control of breathing in birds compared to mammals. *Phys. Reviews*, 58(3):604–655, Jul 1978.

[24] J. Chang, I. Skromne, and R. K. Ho. CDX4 and retinoic acid interact to position the hindbrain-spinal cord transition. *Dev. Biol.*, 410(2):178–189, Feb 2016.

[25] J. D. Clarke, B. P. Hayes, S. P. Hunt, and A. Roberts. Sensory physiology, anatomy and immunohistochemistry of Rohon-Beard neurones in embryos of Xenopus laevis. *J. Physiol. (Lond.)*, 348:511–525, Mar 1984.

[26] E. H. Coolidge, C. S. Ciuhandu, and W. K. Milsom. A comparative analysis of putative oxygen-sensing cells in the fish gill. *J. Exp. Biol.*, 211(Pt 8):1231–1242, Apr 2008.

[27] J. DeFelipe. The dendritic spine story: an intriguing process of discovery. *Front Neuroanat*, 9:14, 2015.

[28] M. Distel, M. F. Wullimann, and R. W. Köster. Optimized Gal4 genetics for permanent gene expression mapping in zebrafish. *Proc. Natl. Acad. Sci. U.S.A.*, 106(32):13365–13370, Aug 2009.

[29] A. Faucherre, J. Nargeot, M. E. Mangoni, and C. Jopling. piezo2b regulates vertebrate light touch response. *J. Neurosci.*, 33(43):17089–17094, Oct 2013.

[30] T. E. Finger. Hierarchical Grouping to Optimize an Objective Function. *J. of the Am. Stat. Assoc.*, 58(301):236–244, Apr 1963.

[31] T. E. Finger. Somatotopy in the representation of the pectoral fin and free fin rays in the spinal cord of the sea robin, Prionotus carolinus. *Biol. Bull.*, 163:154–161, Aug 1982.

[32] T. E. Finger. Ascending spinal systems in the fish, Prionotus carolinus. *J. Comp. Neurol.*, 422(1):106–122, Jun 2000.

[33] P. Gau, J. Poon, C. Ufret-Vincenty, C. D. Snelson, S. E. Gordon, D. W. Raible, and A. Dhaka. The zebrafish ortholog of TRPV1 is required for heat-induced locomotion. *J. Neurosci.*, 33(12):5249–5260, Mar 2013.

[34] A. R. Gehrke, I. Schneider, E. de la Calle-Mustienes, J. J. Tena, C. Gomez-Marin, M. Chandran, T. Nakamura, I. Braasch, J. H. Postlethwait, J. L. Gómez-Skarmeta, and N. H. Shubin. Deep conservation of wrist and digit enhancers in fish. *Proc. Natl. Acad. Sci. U.S.A.*, 112(3):803–808, Jan 2015.

[35] C. Golgi. Sulla struttura della sostanza grigia del cervello. *Gazz. Med. Ita. Lombarda.*, 33:244–246, 1873.

[36] C. Golgi. Sulla Fina Struttura del Bulbi Olfattorii. *Reggio-Emilia Print. Stefano Calderini.*, 1885.

[37] C. Golgi. Sulla fina anatomia degli organi centrali del sistema nervoso. Lettera al Prof. Luigi Luciani La lettera fu pubblicata in parte nel Trattato di fisiologia dell'uomo del Professore Luigi Luciani ordinario di Fisiologia nell Universita di Roma. *Societa e. Opera Omnia*, II:721–733, 1903.

[38] C. Golgi. Sulla fina anatomia degli organi centrali del sistema nervoso. Rivista sperimentale di Freniatria, anni 1882âĂŞ83. *Societa e. Opera Omnia*, I:295–393, 1903.

[39] H. Grandel and S. Schulte-Merker. The development of the paired fins in the zebrafish (Danio rerio). *Mech. Dev.*, 79(1-2):99–120, Dec 1998.

[40] M. H. Green, O. M. Curet, N. A. Patankar, and M. E. Hale. Fluid dynamics of the larval zebrafish pectoral fin and the role of fin bending in fluid transport. *Bioinspir Biomim*, 8(1):016002, Mar 2013.

[41] M. H. Green, R. K. Ho, and M. E. Hale. Movement and function of the pectoral fins of the larval zebrafish (Danio rerio) during slow swimming. *J. Exp. Biol.*, 214(Pt 18):3111–3123, Sep 2011.

[42] W. B. Grueber and A. Sagasti. Self-avoidance and tiling: Mechanisms of dendrite and axon spacing. *Cold Spring Harb Perspect Biol*, 2(9):a001750, Sep 2010.

[43] J. Hachisuka, K. M. Baumbauer, Y. Omori, L. M. Snyder, H. R. Koerber, and S. E. Ross. Semi-intact ex vivo approach to investigate spinal somatosensory circuits. *Elife*, 5, 12 2016.

[44] M. E. Hale. Developmental change in the function of movement systems: transition of the pectoral fins between respiratory and locomotor roles in zebrafish. *Integr. Comp. Biol.*, 54(2):238–249, Jul 2014.

[45] M. E. Hale, D. A. Ritter, and J. R. Fetcho. A confocal study of spinal interneurons in living larval zebrafish. *J. Comp. Neurol.*, 437(1):1–16, Aug 2001.

[46] A. R. Hardy. Exploring the tactile and gustatory capacities of fish fins. [Unpublished doctoral dissertation.]. *Univ. of Chicago*, August 2020.

[47] A. R. Hardy, B. M. Steinworth, and M. E. Hale. Touch sensation by pectoral fins of the catfish Pimelodus pictus. *Proc. Biol. Sci.*, 283(1824), Feb 2016.

[48] M. Haring, A. Zeisel, H. Hochgerner, P. Rinwa, J. E. T. Jakobsson, P. Lonnerberg, G. La Manno, N. Sharma, L. Borgius, O. Kiehn, M. C. Lagerstrom, S. Linnarsson, and P. Ernfors. Neuronal atlas of the dorsal horn defines its architecture and links sensory input to transcriptional cell types. *Nat. Neurosci.*, 21(6):869–880, Jun 2018.

[49] A. C. Hart, J. Kass, J. E. Shapiro, and J. M. Kaplan. Distinct signaling pathways mediate touch and osmosensory responses in a polymodal sensory neuron. *J. Neurosci.*, 19(6):1952–1958, Mar 1999.

[50] K. O. Hartley, S. L. Nutt, and E. Amaya. Targeted gene expression in transgenic Xenopus using the binary Gal4-UAS system. *Proc. Natl. Acad. Sci. U.S.A.*, 99(3):1377–1382, Feb 2002.

[51] M. He, J. Tucciarone, S. Lee, M. J. Nigro, Y. Kim, J. M. Levine, S. M. Kelly, I. Krugikov, P. Wu, Y. Chen, L. Gong, Y. Hou, P. Osten, B. Rudy, and Z. J. Huang. Strategies and Tools for Combinatorial Targeting of GABAergic Neurons in Mouse Cerebral Cortex. *Neuron*, 91(6):1228–1243, Sep 2016.

[52] P. D. Henion, D. W. Raible, C. E. Beattie, K. L. Stoesser, J. A. Weston, and J. S. Eisen. Screen for mutations affecting development of Zebrafish neural crest. *Dev. Genet.*, 18(1):11–17, 1996.

[53] C. Hensey and J. Gautier. Programmed cell death during Xenopus development: a spatio-temporal analysis. *Dev. Biol.*, 203(1):36–48, Nov 1998.

[54] K. Hinsch and G. K. Zupanc. Generation and long-term persistence of new neurons in the adult zebrafish brain: a quantitative analysis. *Neuroscience*, 146(2):679–696, May 2007.

[55] Y. Honjo, J. Kniss, and J. S. Eisen. Neuregulin-mediated ErbB3 signaling is required for formation of zebrafish dorsal root ganglion neurons. *Development*, 135(15):2615–2625, Aug 2008.

[56] K. W. Horch, R. P. Tuckett, and P. R. Burgess. A key to the classification of cutaneous mechanoreceptors. *J. Invest. Dermatol.*, 69(1):75–82, Jul 1977.

[57] J. M. Hubbard, U. L. Bőhm, A. Prendergast, P. B. Tseng, M. Newman, C. Stokes, and C. Wyart. Intraspinal Sensory Neurons Provide Powerful Inhibition to Motor Circuits Ensuring Postural Control during Locomotion. *Curr. Biol.*, 26(21):2841–2853, Nov 2016.

[58] A. Hughes. The development of the primary sensory system in Xenopus laevis (Daudin). *J. Anat.*, 91(3):323–338, Jul 1957.

[59] J. R. Hunter. Swimming and feeding behavior of larval anchovy Engraulis mordax. *Fish. Bull. US*, 70(3):821–838, 1972.

[60] J. R. Hunter and J. R. Zweifel. Swimming speed, tail beat frequency, tail beat amplitude, and size in jack mackerel, Trachurus symmetricus, and other fishes. *Fish. Bull. Fish Wildl. Serv. US*, 69:253–266, 1971.

[61] E. Jacob, M. Drexel, T. Schwerte, and B. Pelster. Influence of hypoxia and of hypoxemia on the development of cardiac activity in zebrafish larvae. *Am. J. Physiol. Regul. Integr. Comp. Physiol.*, 283(4):R911–917, Oct 2002.

[62] B. A. Jenkins and E. A. Lumpkin. Developing a sense of touch. *Development*, 144(22):4078–4090, 11 2017.

[63] M. G. Jonz and C. A. Nurse. Neuroepithelial cells and associated innervation of the zebrafish gill: a confocal immunofluorescence study. *J. Comp. Neurol.*, 461(1):1–17, Jun 2003.

[64] M. G. Jonz and C. A. Nurse. Development of oxygen sensing in the gills of zebrafish. *J. Exp. Biol.*, 208(Pt 8):1537–1549, Apr 2005.

[65] M. G. Jonz and C. A. Nurse. Ontogenesis of oxygen chemoreception in aquatic vertebrates. *Respir Physiol Neurobiol*, 154(1-2):139–152, Nov 2006.

[66] J. M. Kaplan and H. R. Horvitz. A dual mechanosensory and chemosensory neuron in Caenorhabditis elegans. *Proc. Natl. Acad. Sci. U.S.A.*, 90(6):2227–2231, Mar 1993.

[67] H. Katz, E. Menelaou, and M. E. Hale. Morphological and physiological properties of Rohon-Beard neurons along the zebrafish spinal cord. *submitted*, 2020.

[68] C. K. Kim, A. Adhikari, and K. Deisseroth. Integration of optogenetics with complementary methodologies in systems neuroscience. *Nat. Rev. Neurosci.*, 18(4):222–235, 03 2017.

[69] C. B. Kimmel, S. L. Powell, and W. K. Metcalfe. Brain neurons which project to the spinal cord in young larvae of the zebrafish. *J. Comp. Neurol.*, 205(2):112–127, Feb 1982.

[70] M. Kirino, J. Parnes, A. Hansen, S. Kiyohara, and T. E. Finger. Evolutionary origins of taste buds: phylogenetic analysis of purinergic neurotransmission in epithelial chemosensors. *Open Biol*, 3(3):130015, Mar 2013.

[71] S. Knafo, K. Fidelin, A. Prendergast, P. B. Tseng, A. Parrin, C. Dickey, U. L. Bőhm, S. N. Figueiredo, O. Thouvenin, H. Pascal-Moussellard, and C. Wyart. Mechanosensory neurons control the timing of spinal microcircuit selection during locomotion. *Elife*, 6, 06 2017.

[72] J. J. Kollros and V. M. McMurray. The mesencephalic V nucleus in anurans. I. Normal development in Rana pipiens. *J. Comp. Neurol.*, 102(1):47–63, Feb 1955.

[73] J. J. Kollros and M. L. Thiesse. Growth and death of cells of the mesencephalic fifth nucleus in Xenopus laevis larvae. *J. Comp. Neurol.*, 233(4):481–489, Mar 1985.

[74] D. Kőnig, P. Dagenais, A. Senk, V. Djonov, C. M. Aegerter, and A. Jazwinska. Distribution and Restoration of Serotonin-Immunoreactive Paraneuronal Cells During Caudal Fin Regeneration in Zebrafish. *Front Mol Neurosci*, 12:227, 2019.

[75] S. Kucenas, F. Soto, J. A. Cox, and M. M. Voigt. Selective labeling of central and peripheral sensory neurons in the developing zebrafish using P2X(3) receptor subunit transgenes. *J. Neurosci.*, 138(2):641–652, 2006.

[76] E. D. Kuehn, S. Meltzer, V. E. Abraira, C. Y. Ho, and D. D. Ginty. Tiling and somatotopic alignment of mammalian low-threshold mechanoreceptors. *Proc. Natl. Acad. Sci. U.S.A.*, 116(19):9168–9177, 05 2019.

[77] J. E. Lamborghini. Disappearance of Rohon-Beard neurons from the spinal cord of larval Xenopus laevis. *J. Comp. Neurol.*, 264(1):47–55, Oct 1987.

[78] O. Larouche, M. L. Zelditch, and R. Cloutier. Fin modules: an evolutionary perspective on appendage disparity in basal vertebrates. *BMC Biol.*, 15(1):32, 04 2017.

[79] L. Li and D. D. Ginty. The structure and organization of lanceolate mechanosensory complexes at mouse hair follicles. *Elife*, 3:e01901, Feb 2014.

[80] L. Li, M. Rutlin, V. E. Abraira, C. Cassidy, L. Kus, S. Gong, M. P. Jankowski, W. Luo, N. Heintz, H. R. Koerber, C. J. Woodbury, and D. D. Ginty. The functional organization of cutaneous low-threshold mechanosensory neurons. *Cell*, 147(7):1615–1627, Dec 2011.

[81] W. Li, Z. Feng, P. W. Sternberg, and X. Z. Xu. A C. elegans stretch receptor neuron revealed by a mechanosensitive TRP channel homologue. *Nature*, 440(7084):684–687, Mar 2006.

[82] M. Linkert, C. T. Rueden, C. Allan, J. M. Burel, W. Moore, A. Patterson, B. Loranger, J. Moore, C. Neves, D. Macdonald, A. Tarkowska, C. Sticco, E. Hill, M. Rossner, K. W. Eliceiri, and J. R. Swedlow. Metadata matters: access to image data in the real world. *J. Cell Biol.*, 189(5):777–782, May 2010.

[83] Y. C. Liu and M. E. Hale. Local Spinal Cord Circuits and Bilateral Mauthner Cell Activity Function Together to Drive Alternative Startle Behaviors. *Curr. Biol.*, 27(5):697–704, Mar 2017.

[84] M. H. Longair, D. A. Baker, and J. D. Armstrong. Simple Neurite Tracer: open source software for reconstruction, visualization and analysis of neuronal processes. *Bioinformatics*, 27(17):2453–2454, Sep 2011.

[85] O. Lowenstein. Pressure Receptors in the Fins of the Dogfish Scylliorhinus Canicula. *J. Exp. Biol.*, 33(2):417–421, Jun 1956.

[86] L. H. Ma, E. Gilland, A. H. Bass, and R. Baker. Ancestry of motor innervation to pectoral fin and forelimb. *Nat Commun*, 1:49, Jul 2010.

[87] L. H. Ma, B. Punnamoottil, S. Rinkwitz, and R. Baker. Mosaic hoxb4a neuronal pleiotropism in zebrafish caudal hindbrain. *PLoS ONE*, 4(6):e5944, Jun 2009.

[88] E. R. Macagno. Number and distribution of neurons in leech segmental ganglia. *J. Comp. Neurol.*, 190(2):283–302, Mar 1980.

[89] L. Madisen, A. R. Garner, D. Shimaoka, A. S. Chuong, N. C. Klapoetke, L. Li, A. van der Bourg, Y. Niino, L. Egolf, C. Monetti, H. Gu, M. Mills, A. Cheng, B. Tasic, T. N. Nguyen, S. M. Sunkin, A. Benucci, A. Nagy, A. Miyawaki, F. Helmchen, R. M. Empson, T. Kn?pfel, E. S. Boyden, R. C. Reid, M. Carandini, and H. Zeng. Transgenic mice for intersectional targeting of neural sensors and effectors with high specificity and performance. *Neuron*, 85(5):942–958, Mar 2015.

[90] E. Menelaou, C. VanDunk, and D. L. McLean. Differences in the morphology of spinal V2a neurons reflect their recruitment order during swimming in larval zebrafish. *J. Comp. Neurol.*, 522(6):1232–1248, Apr 2014.

[91] W. K. Metcalfe, P. Z. Myers, B. Trevarrow, M. B. Bass, and C. B. Kimmel. Primary neurons that express the L2/HNK-1 carbohydrate during early development in the zebrafish. *Development*, 110(2):491–504, Oct 1990.

[92] M. R. Miller, H. J. Ralston, and M. Kasahara. The pattern of cutaneous innervation of the human hand. *Am. J. Anat.*, 102(2):183–217, Mar 1958.

[93] E. M. Morin-Kensicki, E. Melancon, and J. S. Eisen. Segmental relationship between somites and vertebral column in zebrafish. *Development*, 129(16):3851–3860, Aug 2002.

[94] A. D. Morrill. The pectoral appendages of Prionotus and their innervation. *J. of Morph.*, 11(1):177–192, May 1895.

[95] A. Muñoz, M. Muñoz, A. Gonzalez, and H. J. ten Donkelaar. Spinal ascending pathways in amphibians: cells of origin and main targets. *J. Comp. Neurol.*, 378(2):205–228, Feb 1997.

[96] Y. Murata, M. Tamura, Y. Aita, K. Fujimura, Y. Murakami, M. Okabe, N. Okada, and M. Tanaka. Allometric growth of the trunk leads to the rostral shift of the pelvic fin in teleost fishes. *Dev. Biol.*, 347(1):236–245, Nov 2010.

[97] P. Z. Myers. Spinal motoneurons of the larval zebrafish. *J. Comp. Neurol.*, 236(4):555–561, Jun 1985.

[98] T. Nakamura, A. R. Gehrke, J. Lemberg, J. Szymaszek, and N. H. Shubin. Digits and fin rays share common developmental histories. *Nature*, 537(7619):225–228, 09 2016.

[99] T. Nakao and A. Ishizawa. Development of the spinal nerves in the lamprey: I. Rohon-Beard cells and interneurons. *J. Comp. Neurol.*, 256(3):342–355, Feb 1987.

[100] N. L. Neubarth, A. J. Emanuel, Y. Liu, M. W. Springel, A. Handler, Q. Zhang, B. P. Lehnert, C. Guo, L. L. Orefice, A. Abdelaziz, M. M. DeLisle, M. Iskols, J. Rhyins, S. J. Kim, S. J. Cattel, W. Regehr, C. D. Harvey, J. Drugowitsch, and D. D. Ginty. Meissner corpuscles and their spatially intermingled afferents underlie gentle touch perception. *Science*, 368(6497), 06 2020.

[101] H. F. Nijhout. Stretch-induced moulting in Oncopeltus fasciatus. *J. Insect Phys.*, 25(3):277–281, Oct 1978.

[102] E. Olesnicky, L. Hernandez-Lagunas, and K. B. Artinger. prdm1a Regulates sox10 and islet1 in the development of neural crest and Rohon-Beard sensory neurons. *Genesis*, 48(11):656–666, Nov 2010.

[103] W. Olson, P. Dong, M. Fleming, and W. Luo. The specification and wiring of mammalian cutaneous low-threshold mechanoreceptors. *Wiley Interdiscip Rev Dev Biol*, 5(3):389–404, 2016.

[104] A. M. Palanca, S. L. Lee, L. E. Yee, C. Joe-Wong, l. e. A. Trinh, E. Hiroyasu, M. Husain, S. E. Fraser, M. Pellegrini, and A. Sagasti. New transgenic reporters identify somatosensory neuron subtypes in larval zebrafish. *Dev Neurobiol*, 73(2):152–167, Feb 2013.

[105] Y. A. Pan, M. Choy, D. A. Prober, and A. F. Schier. Robo2 determines subtype-specific axonal projections of trigeminal sensory neurons. *Development*, 139(3):591–600, Feb 2012.

[106] M. Paré, A. M. Smith, and F. L. Rice. Distribution and terminal arborizations of cutaneous mechanoreceptors in the glabrous finger pads of the monkey. *J. Comp. Neurol.*, 445(4):347–359, Apr 2002.

[107] A. A. Patel and D. N. Cox. Behavioral and Functional Assays for Investigating Mechanisms of Noxious Cold Detection and Multimodal Sensory Processing in Drosophila Larvae. *Bio Protoc*, 7(13), Jul 2017.

[108] S. E. Patterson, L. B. Mook, and S. H. Devoto. Growth in the larval zebrafish pectoral fin and trunk musculature. *Dev. Dyn.*, 237(2):307–315, Feb 2008.

[109] E. R. Perl. Function of dorsal root ganglion neurons: an overview. *Sensory Neurons: Diversity, Development, and Plasticity*, pages 3–23, 1992.

[110] R. H. Pineda, R. A. Heiser, and A. B. Ribera. Developmental, molecular, and genetic dissection of INa in vivo in embryonic zebrafish sensory neurons. *J. Neurophysiol.*, 93(6):3582–3593, Jun 2005.

[111] A. J. Pittman, M. Y. Law, and C. B. Chien. Pathfinding in a large vertebrate axon tract: isotypic interactions guide retinotectal axons at multiple choice points. *Development*, 135(17):2865–2871, Sep 2008.

[112] C. S. Porteus, D. L. Brink, and W. K. Milsom. Neurotransmitter profiles in fish gills: putative gill oxygen chemoreceptors. *Respir Physiol Neurobiol*, 184(3):316–325, Dec 2012.

[113] V. E. Prince, L. Joly, M. Ekker, and R. K. Ho. Zebrafish hox genes: genomic organization and modified colinear expression patterns in the trunk. *Development*, 125(3):407–420, Feb 1998.

[114] D. A. Prober, S. Zimmerman, B. R. Myers, B. M. McDermott, S. H. Kim, S. Caron, J. Rihel, L. Solnica-Krezel, D. Julius, A. J. Hudspeth, and A. F. Schier. Zebrafish TRPA1 channels are required for chemosensation but not for thermosensation or mechanosensory hair cell function. *J. Neurosci.*, 28(40):10102–10110, Oct 2008.

[115] D. W. Raible, A. Wood, W. Hodsdon, P. D. Henion, J. A. Weston, and J. S. Eisen. Segregation and early dispersal of neural crest cells in the embryonic zebrafish. *Dev. Dyn.*, 195(1):29–42, Sep 1992.

[116] S. Ramón y Cajal. Estructura de los centros nerviosos de las aves. *Rev. Trim. Histol. Norm. Pat.*, 1:1–10, 1888.

[117] S. Ramón y Cajal. Estructura del asta de Ammon y fascia dentate. *An. Soc. Esp. Hist. Nat.*, 22:53–114, 1893.

[118] S. Ramón y Cajal. La fine structure des centres nerveux. The croonian lecture. *Proc. R. Soc. Lond. B Biol. Sci.*, 55:443–468, 1894.

[119] K. S. Regan, M. G. Jonz, and P. A. Wright. Neuroepithelial cells and the hypoxia emersion response in the amphibious fish Kryptolebias marmoratus. *J. Exp. Biol.*, 214(Pt 15):2560–2568, Aug 2011.

[120] R. Reyes, M. Haendel, D. Grant, E. Melancon, and J. S. Eisen. Slow degeneration of zebrafish Rohon-Beard neurons during programmed cell death. *Dev. Dyn.*, 229(1):30–41, Jan 2004.

[121] F. L. Rice and P. J. Albrecht. 6.01 - Cutaneous Mechanisms of Tactile Perception: Morphological and Chemical Organization of the Innervation to the Skin. *The Senses: A Comprehensive Reference*, pages 287–315, Dec 1973.

[122] R. M. A. P. Ridge. Physiological responses of stretch receptors in the pectoral fin of the ray Raja clavata. *"Journal of the Marine Biological Association of the United Kingdom"*, 57(2):535–541, May 1977.

[123] A. Roberts and B. P. Hayes. The anatomy and function of 'free' nerve endings in an amphibian skin sensory system. *Proc. R. Soc. Lond., B, Biol. Sci.*, 196(1125):415–429, Apr 1977.

[124] V. Rohon. Zur Histogenese des Riickenmarkes der Forelle. *S.B. bayer. Akad. Wiss. Math.*, 14:39–57, 1885.

[125] P. Rombough. Gills are needed for ionoregulation before they are needed for O2 uptake in developing zebrafish, Danio rerio. *J. Exp. Biol.*, 205(Pt 12):1787–1794, Jun 2002.

[126] M. Ronan and R. G. Northcutt. Projections ascending from the spinal cord to the brain in petromyzontid and myxinoid agnathans. *J. Comp. Neurol.*, 291(4):491–508, Jan 1990.

[127] RStudio Team. Rstudio: Integrated development environment for r. *RStudio, PBC.*, 2020.

[128] A. Sagasti, M. R. Guido, D. W. Raible, and A. F. Schier. Repulsive interactions shape the morphologies and functional arrangement of zebrafish peripheral sensory arbors. *Curr. Biol.*, 15(9):804–814, May 2005.

[129] Y. Sato, S. Nakajima, N. Shiraga, H. Atsumi, S. Yoshida, T. Koller, G. Gerig, and R. Kikinis. Three-dimensional multi-scale line filter for segmentation and visualization of curvilinear structures in medical images. *Med Image Anal*, 2(2):143–168, Jun 1998.

[130] J. Schindelin, I. Arganda-Carreras, E. Frise, V. Kaynig, M. Longair, T. Pietzsch, S. Preibisch, C. Rueden, S. Saalfeld, B. Schmid, J. Y. Tinevez, D. J. White, V. Hartenstein, K. Eliceiri, P. Tomancak, and A. Cardona. Fiji: an open-source platform for biological-image analysis. *Nat. Methods*, 9(7):676–682, Jun 2012.

[131] C. A. Schneider, W. S. Rasband, and K. W. Eliceiri. NIH Image to ImageJ: 25 years of image analysis. *Nat. Methods*, 9(7):671–675, Jul 2012.

[132] J. W. Sensinger and S. Dosen. A Review of Sensory Feedback in Upper-Limb Prostheses From the Perspective of Human Motor Control. *Front Neurosci*, 14:345, 2020.

[133] B. Sharif, A. R. Ase, A. Ribeiro-da Silva, and P. Séguéla. Differential Coding of itch and pain by a subpopulation of primary afferent neurons. *Neuron*, 106(6):940–951, Jun 2020.

[134] K. T. Sillar and A. Roberts. Unmyelinated cutaneous afferent neurons activate two types of excitatory amino acid receptor in the spinal cord of Xenopus laevis embryos. *J. Neurosci.*, 8(4):1350–1360, Apr 1988.

[135] W. L. Silver and Finger T. E. Electrophysiological examination of a non-olfactory, non-gustatory chemosense in the searobin, Prionotus carolinus. *J. Comp. Physiol.*, 154:167–174, Mar 1984.

[136] M. G. Simões, A. Bensimon-Brito, M. Fonseca, A. Farinho, F. Val?rio, S. Sousa, N. Afonso, A. Kumar, and A. Jacinto. Denervation impairs regeneration of amputated zebrafish fins. *BMC Dev. Biol.*, 14:49, Dec 2014.

[137] M. A. Simon and B. A. Trimmer. Movement encoding by a stretch receptor in the soft-bodied caterpillar, Manduca sexta. *J. Exp. Biol.*, 212(Pt 7):1021–1031, Apr 2009.

[138] I. Skromne, D. Thorsen, M. Hale, V. E. Prince, and R. K. Ho. Repression of the hindbrain developmental program by Cdx factors is required for the specification of the vertebrate spinal cord. *Development*, 134(11):2147–2158, Jun 2007.

[139] Y. Takahashi and Y. Nakajima. Dermatomes in the rat limbs as determined by antidromic stimulation of sensory C-fibers in spinal nerves. *Pain*, 67(1):197–202, Sep 1996.

[140] D. A. Tamarkin and R. B. Levine. Synaptic interactions between a muscle-assocaiated proprioceptor and body wall muscle motor neurons in larval and adult Manduca sexta. *J. Neurophys.*, 76(3):1597–1610, Sep 1996.

[141] J. S. Taylor and A. Roberts. The early development of the primary sensory neurones in an amphibian embryo: a scanning electron microscope study. *J Embryol Exp Morphol*, 75:49–66, Jun 1983.

[142] D. H. Thorsen, J. J. Cassidy, and M. E. Hale. Swimming of larval zebrafish: fin-axis coordination and implications for function and neural control. *J. Exp. Biol.*, 207(Pt 24):4175–4183, Nov 2004.

[143] D. H. Thorsen and M. E. Hale. Development of zebrafish (Danio rerio) pectoral fin musculature. *J. Morphol.*, 266(2):241–255, Nov 2005.

[144] D. H. Thorsen and M. E. Hale. Neural development of the zebrafish (Danio rerio) pectoral fin. *J. Comp. Neurol.*, 504(2):168–184, Sep 2007.

[145] K. Umeda, T. Ishizuka, H. Yawo, and W. Shoji. Position- and quantity-dependent responses in zebrafish turning behavior. *Sci Rep*, 6:27888, 06 2016.

[146] D. Weihs. Respiration and depth control as possible reasons for swimming of northern anchovy, Engraulis mordax, yolk-sac larvae. *Fish. Bull. US*, 78(1):109–117, 1980.

[147] I. R. Wickersham, D. C. Lyon, R. J. Barnard, T. Mori, S. Finke, K. K. Conzelmann, J. A. Young, and E. M. Callaway. Monosynaptic restriction of transsynaptic tracing from single, genetically targeted neurons. *Neuron*, 53(5):639–647, Mar 2007.

[148] H. Wickham. ggplot2 elegant graphics for data analysis (Use R!). *Springer*, 2016.

[149] J. A. Williams, A. Barrios, C. Gatchalian, L. Rubin, S. W. Wilson, and N. Holder. Programmed cell death in zebrafish rohon beard neurons is influenced by TrkC1/NT-3 signaling. *Dev. Biol.*, 226(2):220–230, Oct 2000.

[150] R. Williams and M. E. Hale. Fin ray sensation participates in the generation of normal fin movement in the hovering behavior of the bluegill sunfish (Lepomis macrochirus). *J. Exp. Biol.*, 218(Pt 21):3435–3447, Nov 2015.

[151] R. Williams, N. Neubarth, and M. E. Hale. The function of fin rays as proprioceptive sensors in fish. *Nat Commun*, 4:1729, 2013.

[152] R. W. Williams and K. Herrup. The control of neuron number. *Annu. Rev. Neurosci.*, 11:423–453, 1988.

[153] Y. J. Won, F. Ono, and S. R. Ikeda. Characterization of Na+ and Ca2+ channels in zebrafish dorsal root ganglion neurons. *PLoS ONE*, 7(8):e42602, 2012.

[154] Y. Yokota and R. M. Bradley. Geniculate Ganglion Neurons are Multimodal and Variable in Receptive Field Characteristics. *Neuroscience*, 367:147–158, Dec 2017.

[155] K. Yoshida, K. Kawakami, G. Abe, and K. Tamura. Zebrafish can regenerate endoskeleton in larval pectoral fin but the regenerative ability declines. *Dev. Biol.*, 463(2):110–123, Jul 2020.

[156] G. Zaccone, E. R. Lauriano, G. Capillo, and M. Kuciel. Air- breathing in fish: Air- breathing organs and control of respiration: Nerves and neurotransmitters in the air-breathing organs and the skin. *Acta Histochem.*, 120(7):630–641, Oct 2018.

[157] G. Zaccone, E. R. Lauriano, M. Kuciel, G. Capillo, S. Pergolizzi, A. Alesci, A. Ishimatsu, Y. K. Ip, and J. M. Icardo. Identification and distribution of neuronal nitric oxide synthase and neurochemical markers in the neuroepithelial cells of the gill and the skin in the giant mudskipper, Periophthalmodon schlosseri. *Zoology (Jena)*, 125:41–52, 12 2017.

[158] P. C. Zachar, W. Pan, and M. G. Jonz. Distribution and morphology of cholinergic cells in the branchial epithelium of zebrafish (Danio rerio). *Cell Tissue Res.*, 367(2):169–179, 02 2017.

[159] N. Zampieri, T. M. Jessell, and A. J. Murray. Mapping sensory circuits by anterograde transsynaptic transfer of recombinant rabies virus. *Neuron*, 81(4):766–778, Feb 2014.

[160] T. A. Zelenchuk and J. L. Brusés. In vivo labeling of zebrafish motor neurons using an mnx1 enhancer and Gal4/UAS. *Genesis*, 49(7):546–554, Jul 2011.

[161] B. Zingg, X. L. Chou, Z. G. Zhang, L. Mesik, F. Liang, H. W. Tao, and L. I. Zhang. AAV-Mediated Anterograde Transsynaptic Tagging: Mapping Corticocollicular Input-Defined Neural Pathways for Defense Behaviors. *Neuron*, 93(1):33–47, Jan 2017.

[162] S. L. Zipursky and W. B. Grueber. The molecular basis of self-avoidance. *Annu. Rev. Neurosci.*, 36:547–568, Jul 2013.

[163] G. K. Zupanc, K. Hinsch, and F. H. Gage. Proliferation, migration, neuronal differentiation, and long-term survival of new cells in the adult zebrafish brain. *J. Comp. Neurol.*, 488(3):290–319, Aug 2005.